Multi-scale analysis of ageing behaviour in bituminous materials

Khalighi, Sadaf; Ma, Lili; Primerano, Kristina; Mirwald, Johannes; Hofko, Bernhard; van Lent, Diederik; Varveri, Aikaterini

DOI
10.1080/14680629.2025.2487210

Publication date
2025

Document Version
Final published version

Published in
Road Materials and Pavement Design

Road Materials and Pavement Design

ISSN: (Print) (Online) Journal homepage: www.tandfonline.com/journals/trmp20

Multi-scale analysis of ageing behaviour in bituminous materials

Sadaf Khalighi, Lili Ma, Kristina Primerano, Johannes Mirwald, Bernhard Hofko, Diederik van Lent & Aikaterini Varveri

To cite this article: Sadaf Khalighi, Lili Ma, Kristina Primerano, Johannes Mirwald, Bernhard Hofko, Diederik van Lent & Aikaterini Varveri (14 Apr 2025): Multi-scale analysis of ageing behaviour in bituminous materials, Road Materials and Pavement Design, DOI: 10.1080/14680629.2025.2487210

To link to this article: https://doi.org/10.1080/14680629.2025.2487210

Published online: 14 Apr 2025.

ROAD MATERIALS AND PAVEMENT DESIGN
https://doi.org/10.1080/14680629.2025.2487210

Taylor & Francis
Taylor & Francis Group

Multi-scale analysis of ageing behaviour in bituminous materials

Sadaf Khalighi[a], Lili Ma[a], Kristina Primerano [b], Johannes Mirwald [b], Bernhard Hofko [b], Diederik van Lent[c] and Aikaterini Varveri [a]

[a]Pavement Engineering, Structure Engineering, Delft University of Technology, Delft, The Netherlands; [b]Christian Doppler Laboratory for Chemo-Mechanical Analysis of Bituminous Materials, Institute of Transportation, TU Wien, Austria; [c]Netherlands Organizations for Applied Scientific Research (TNO), Delft, The Netherlands

ABSTRACT

Understanding aging across material scales is critical for predicting the long-term performance of bituminous materials. This study investigates the aging of binder, mastic, and asphalt mixture samples under various temperature, pressure, reactive oxygen species (ROS), and humidity. Chemical aging processes were analysed using attenuated total reflectance Fourier-transform infrared spectroscopy (ATR-FTIR), principal component analysis (PCA), and Euclidean distance. Normalisation, baseline correction, and advanced ATR correction were used to enhance the accuracy of FTIR results. Hydrated lime in mastics enhanced the resistance to oxidative aging, particularly under hygrothermal conditions. PCA identified key spectral regions for understanding aging processes of bituminous materials. Porous asphalt (PA) mixtures aged more than stone mastic asphalt under field-like conditions. PCA identified distinct aging clusters at low and high pressure. Euclidean distance analysis indicated that binder-level aging can approximate mastic and mixture aging under certain conditions. The findings confirm that FTIR indices are effective for multi-scale aging studies.

ARTICLE HISTORY
Received 28 October 2024
Accepted 23 March 2025

KEYWORDS
Aging; Multi-scale; Bitumen; Mastic; Mixture; Chemometrics

1. Introduction

The aging process of bituminous binders is a critical factor in determining the lifespan of asphalt pavements, as excessive aging significantly affects the durability of asphalt mixtures. Aging occurs in two phases: short-term aging, which takes place during processes like storage, mixing, and paving at elevated temperatures, and long-term aging, which happens in-service (Petersen, 2009). Key mechanisms, driving these aging processes include as oxidation, evaporation of volatile components, and steric hindrance. Among these, oxidative aging has a particularly strong impact on the long-term performance of pavements, making it essential to evaluate binder performance under laboratory conditions that accurately simulate field aging to ensure optimal pavement durability (Hofer et al., 2023).

Standard aging protocols have been developed for bituminous binders and mastics, including methods such as the Rolling Thin Film Oven (RTFO) and Thin Film Oven (TFO) for short-term aging, and the Pressure Aging Vessel (PAV) for long-term aging (Hofko & Hospodka, 2016; Koyun et al., 2022; Nagabhushanarao & Vijayakumar, 2021). RTFO subjects binder films to a controlled airflow at 163°C for 75 min, while TFO involves aging binder films at 163°C for 5 h (EN, 12607-1, 2014). The PAV method subjects binders to 2.07 MPa of pressure at temperatures ranging from 90-110°C for 20 h to simulate

CONTACT Sadaf Khalighi s.khalighi@tudelft.nl

long-term aging (EN, 14769, 2012). For asphalt mixtures, long-term aging is typically conducted using extended oven aging at 85°C for 5 days (Highways & Officials, 1994) or through low-pressure oxidation, conducted in a forced draft oven at 85°C for 5 days with an oxygen flow of 1.9 L/min (Airey, 2003). While these tests provide valuable insights, they do not fully mimic the complex field conditions experienced by asphalt mixtures.

To bridge this gap, efforts are being made to refine laboratory aging protocols to better simulate field aging conditions. Since binders in actual pavement structures interact with mineral fillers and aggregates, it is essential to understand how aging behaviour differs between binders alone and binders within mixtures or mastics. Multi-scale comparisons of aging behaviour—between binders, mastics, and asphalt mixtures—are crucial for gaining a comprehensive understanding of these effects. Environmental factors such as temperature, pressure, moisture, and reactive oxygen species (ROS) also play a significant role in aging (Khalighi et al., 2025b; khalighi et al., 2025a), and their impact on different scales must be carefully studied to develop more representative aging protocols.

Fillers play a significant role in the aging behaviour of asphalt binders by influencing both the chemical and physical properties of asphalt mastics. Anderson et al. (Anderson et al., 1992) emphasised that fine mineral fillers dominate the physicochemical interactions with bitumen, given their large surface area. Studies by Alfaqawi et al. (Alfaqawi et al., 2022) demonstrated that hydrated lime effectively retards aging more than granite fillers, while Gubler et al. (Gubler et al., 1999) noted that fillers can slow down binder aging by obstructing oxygen diffusion. Recasens et al. (Recasens et al., 2005) showed that fillers such as calcium carbonate and hydrated lime reduce the aging effects, particularly by limiting increases in viscosity and softening point. Furthermore, Plancher et al. (Plancher et al., 1976) revealed that hydrated lime reduces oxidative hardening by interacting with oxidation products. Other studies, such as those by Moraes et al. (Moraes & Bahia, 2015) and Wu et al. (Wu et al., 2021), demonstrated that fillers influence molecular size distribution during aging and catalyse oxidation, respectively, affecting the stiffness of asphalt mastics. These findings highlight the complex interaction between fillers and asphalt, with filler type, concentration, and surface properties playing a critical role in aging processes.

The long-term aging (LTA) of asphalt mixtures is more complex than that of mastics due to the presence of aggregates, which contribute to the specific morphology of the mixtures. After construction, LTA in the field begins with the oxidation of bitumen at the pavement surface, as air flows through the interconnected voids into deeper layers of the pavement structure (Jing et al., 2019). This process is highly dependent on the type of asphalt mixture (Erkens et al., 2016), with a clear relationship between air void content and aging sensitivity (Oliver & Tredrea, 1997). Porous asphalt (PA) mixtures exhibit a higher degree of aging compared to dense asphalt mixtures like stone mastic asphalt (SMA) (Schmidt, 1973). The reason behind the different aging sensitivity is the high air void content in PA mixtures, as revealed by CT scan results in previous studies (Jing et al., 2019). This contributes to the interconnectivity of the void network, with over 90% of air voids being interconnected, compared to less than 10% in SMA mixtures (Varveri et al., 2014). This high interconnectivity allows oxygen to penetrate deeper into the PA mixture, resulting in a more pronounced aging gradient throughout the structure. In contrast, SMA mixtures, with their low porosity, experience aging primarily at the surface, where oxygen penetration is slower.

Aside from inherent properties of samples, environmental aging factors are also important for aging studies. Temperature is critical; higher temperatures accelerate oxidation, yet many laboratory protocols exceed realistic pavement conditions (Jing, 2019; Petersen, 2009). This study focuses on moderate temperatures (60°C, 70°C, and 85°C) to better simulate natural aging pathways. Pressure also plays a significant role by influencing oxygen diffusion into binders; experiments often use 20 bar, but this study compares aging under 1 and 150 bar (Jing, 2019). Moisture affects binder properties such as density and viscosity (Ma et al., 2023a), with hygrothermal aging accelerating the process compared to thermo-oxidative aging alone (Khalighi et al., 2024a; Khalighi et al., 2024b). However, moisture must be controlled to avoid limiting oxygen availability. Reactive oxygen species (ROS) like ozone (O_3) and nitrogen oxides (NO_x) significantly impact aging; while studies on ROS effects are limited, methods like the Viennese Binder Aging (VBA) expose binders to these species at 80°C and 1 bar, revealing notable

aging effects (Hofko et al., 2020; Mirwald et al., 2020; Singh et al., 2022). Moreover, adding moisture to VBA accelerates aging (Khalighi et al., 2025b). The Viennese Aging Procedure (VAPro) is another method that ages compacted mixtures at 60°C and loose mixtures at 95°C, showing 1.2 to 2.6 times stronger aging effects compared to the PAV method (Maschauer et al., 2022; Maschauer et al., 2023; Sreeram et al., 2021).

For monitoring aging-related chemical changes in bituminous materials, a widely used technique is Fourier-transform infrared spectroscopy (FTIR) (Hofko et al., 2018; Hu et al., 2022; Khalighi et al., 2024c; Nivitha et al., 2016; Zhang et al., 2024). Depending on how the infrared light interacts with the sample, FTIR can be performed using two methods: transmission and attenuated total reflectance (ATR). In transmission mode, light passes directly through the sample, and the pathlength is defined by the sample thickness and remains constant throughout the spectrum. In contrast, the light interacts with the sample surface and is then reflected back into the detector in the ATR mode. The depth of infrared beam penetration into the sample thus varies with wavelength, the angle of incidence, the refractive indices of the ATR crystal, and the sample. As a result, compared to the transmission mode, the infrared spectrum obtained using the ATR accessory presents distortions in the intensities of specific absorption bands, as well as a shift of these bands to lower frequencies. Detailed explanations and relevant equations can be found in the literature (Simon Nunn, 2008).

To address these issues, an advanced ATR correction algorithm can be applied to compensate for distortions in relative band intensities due to wavelength-dependent penetration depth, shifts in band positions caused by refractive index dispersion, and deviations from Beer's Law arising from non-polarization effects. Several studies have highlighted the importance of applying ATR corrections, particularly for quantitative analyses (e.g. concentration determinations of specific compounds), as uncorrected variables can result in inaccurate measurements and potentially misleading conclusions (Mayerhöfer et al., 2022).

Moreover, the complexity of the resulting data requires advanced techniques for interpretation. To address this, multivariate analysis, including principal component analysis (PCA) and pairwise Euclidean distance, was employed. Previous studies in pavement engineering have demonstrated the effectiveness of PCA in distinguishing aging stages and binder types based on FTIR spectra (Wang et al., 2018) or rheological data(Siroma et al., 2021). Weigel and Stephan (Weigel & Stephan, 2017) explored the use of FTIR spectra and its first derivative for PCA-linear discriminant analysis (LDA) and other regression models, demonstrating that bituminous binder samples, despite differences in grade and aging state, could be accurately distinguished based on refinery origin. Similarly, Ren et al used PCA-LDA to distinguish between asphalt samples from these three oil sources with high accuracy (Ren et al., 2019). Ma et al. utilised PCA-linear discriminant analysis (LDA) to classify binders at various aging stages, while Primerano et al. identified key wavenumbers for classifying aging conditions using multivariate analysis (Ma et al., 2023b; Primerano et al., 2023). Moreover, Motevalizadeh et al. expanded the use of PCA in combination with hierarchical clustering analysis (HCA) to cluster mastic samples into different groups based on their filler types (Motevalizadeh & Mollenhauer, 2024). These techniques provide a robust framework for the present study's analysis of aging in bituminous systems at multiple scales.

2. Objectives

The key research questions addressed by this analysis are:

(1) How do bituminous samples at mastics (with hydrated lime or limestone) and mixtures (PA or SMA) levels respond to various aging factors compared to binder samples?
(2) Can FTIR indices effectively characterise and compare the ageing behaviour at binder, mastic, and mixture levels?
(3) Is it possible to identify closely matching aging conditions across binder, mastic, and mixture scales?

Table 1. Properties of Q 70/100 at fresh (unaged) state.

Property		Unit	Q PEN 70/100
Penetration at 25 °C		0.1 mm	70–100
Softening point		°C	43–51
Complex shear modulus at 1.6 Hz & 60 °C		kPa	1.8
Phase angle at 1.6 Hz & 60 °C		°	88
Elemental composition	Nitrogen N	(%)	0.59
	Carbon C		79.19
	Hydrogen H		10.81
	Sulfur S		4.47
	Oxygen O		2.25

3. Methodology

The objectives of this study are to investigate and compare the aging behaviour of bituminous binders, mastics, and mixtures under various environmental conditions. Specifically, the study is divided into two sections: one focusing on comparing binders and mastics and the other on the comparison between binders and mixtures.

All samples were tested in three states: unaged (fresh), short-term aging (STA), and long-term aging (LTA). For binder-mastic comparison, the Viennese Binder Aging (VBA) method was applied under dry and wet conditions to simulate LTA, exposing samples to ozone and nitrogen dioxide with and without humidity. For binder-mixture comparison, LTA conditions were simulated by varying temperature, humidity, and pressure to assess accelerated aging effects.

Since in this study, FTIR serves as the primary analytical tool, to facilitate the analysis of aging in next steps, we have implemented essential pre-processing techniques, including baseline correction, normalisation, and advanced Attenuated Total Reflectance (ATR) correction. The rationale for employing these methods is thoroughly discussed.

The study employs principal component analysis (PCA) and pairwise distance calculations to evaluate the degree of similarity between aging conditions at different scales. This approach aims to identify key FTIR regions relevant for aging at different scales and to assess the impact of fillers on aging resistance.

4. Materials and methods

4.1. Materials

Binder PEN 70/100 is one of the most used bituminous binders for road construction. In this study, one PEN 70/100 bituminous binder was evaluated, named as Q. Table 1 shows the basic properties of the binder. The specifications for the fillers, namely Wigro (limestone, W) and Wigro60k (hydrated lime, W60k), along with the gradation of aggregates, are detailed in Supporting Information Tables 1S to 3S.

4.2. Samples preparation

Binder samples were prepared by pouring 50 grams of fresh binder onto pans, resulting in films of 3.2 mm thickness. Short-term aging was performed in an oven at 163°C for 5 h following the EN 12607-2 standard [1]. After short-term aging, the STA binder was thoroughly mixed to ensure homogeneity before proceeding with further experimental steps. This homogenisation process is essential to eliminate any oxidation gradients that may have developed due to the surface-dominated aging mechanism of TFOT. By thoroughly mixing the binder, we ensure that any variations in oxidative aging are evenly distributed throughout the sample, preventing localised differences that could influence subsequent analyses. This step enhances the reproducibility and reliability of the results, ensuring that the aged binder used for further testing accurately represents a uniformly aged material. After

short-term aging, the long-term aging process was conducted by carefully transferring portions of the short-term aged binder to glass petri dishes. The specific weight of the STA binder was calculated based on its density and the surface area of the petri dish to ensure consistency across samples. The binder was then spread evenly to achieve a uniform film thickness of 1 mm (Khalighi et al., 2024d). This thickness was confirmed by reheating the samples at 163°C for 3 min. After aging, the binder was carefully removed from the petri dishes by gently warming them.

For mastics, two types of mastic samples were prepared by adding different active fillers: Wigro (limestone, W) and Wigro60k (hydrated lime, W60k). Mastic samples were prepared with a filler-to-bitumen mass ratio of 1 (f/b = 1). A mass-based filler-to-binder (f/b) ratio was chosen to incorporate fillers into the binder to align our study with real-world practices, where fillers are typically added to asphalt mixtures based on mass. The fillers were pre-heated to 130°C before being mixed with bitumen. Bitumen was preheated to 130°C for one hour as well. After adding the required amount of mineral filler to the heated bitumen, the mixture was stirred for five minutes to achieve homogeneity. The resulting mastic was placed in the oven at 130°C for 30 min to enhance bonding, followed by manual stirring to ensure uniform distribution of filler particles.

Binder extraction from the mastic sample was conducted using the micro-extraction method developed in (Filonzi et al., 2020). A small mastic sample was stirred with toluene for 12 h under reduced oxygen conditions to minimise oxidation. The binder-toluene solution was then filtered through a glass syringe filter under vacuum to isolate the binder. To prevent unwanted oxidative aging, the excess solvent was evaporated from the extracted binder solution under a nitrogen flow at room temperature. In this study, small quantities of binder solution in toluene were used, and due to its liquid nature, it spread naturally over a large surface area to form a thin layer. This setup facilitated efficient toluene evaporation at room temperature over an overnight period under nitrogen gas. The complete removal of toluene was confirmed through FTIR analysis (Figure 1S), which showed the disappearance of toluene's characteristic peaks in the spectrum. The absence of filler residues in the extracted binders was verified by analysing their FTIR spectra after the extraction process. No additional peaks were observed in the hydroxyl and long-chain regions, which are typically indicative of mineral filler presence (Figure 1S).

Two types of asphalt mixtures, porous asphalt (PA) and stone mastic asphalt (SMA), were prepared. These mixtures are commonly used in national highways and provincial roads in the Netherlands (Jing et al., 2022). Asphalt mixture samples were prepared using Norwegian sandstone with a nominal maximum size of 16 mm and target air void contents of 16% and 5% for PA and SMA mixtures, respectively. Q binder contents were set at 5.0% and 6.4% for the PA and SMA mixtures, respectively. Table 3S provides details on the mix design and aggregate gradation of these mixtures. Preheating of the granular materials and binder was conducted at 165°C and 150°C, respectively, followed by mixing in a batch mixer, ensuring homogeneity by a sequential addition of materials and binder according to a detailed procedure. Table 4S presents the specific mixing procedure followed in this study. Cellulose fibres were added for PA mixtures. The mixture specimens were prepared as $5 \times 5 \times 5\ cm^3$ cubes, and compacted samples were used for the aging experiments. These samples were utilised for both high-pressure aging and climate chamber aging. The whole specimen was utilised for binder recovery after aging, without any layering. While the potential aging gradient in compacted specimens is recognised, it was not a focus of this study and will be addressed in future work.

Following artificial aging, binders were extracted from the aged asphalt mixture cores using a cold extraction method with dichloromethane, and the binder was recovered via rotary evaporation in accordance with EN 12697-1:2012 and EN 12697-3:2013 standards.

4.3. Long-term aging conditions

Table 2 outlines the aging conditions for binder and mastic samples. To compare the ageing at binder and mastic scales, the Viennese Binder Aging (VBA) method [21] was applied, exposing samples to air enriched with 25 ppm NO_2 and $4\ g/m^3$ ozone at 85 ± 1°C for three days (VBA-Dry) (Mirwald et al.,

Table 2. Aging conditions for binder and mastic samples.

Sample	Thickness/type	Temperature	Pressure	Time	Other aging factors	# of samples & names
Binder	1 mm	85°C	1bar	3 days	NO_2 + ozone + 0 or 20% relative humidity	2 (Q-VBA-Wet) 4 (W-VBA- Wet & exW-VBA- Wet)
Mastic	W, W60k					

Table 3. Aging conditions for binder and mixture samples.

Sample	Thickness/type	Temperature	Pressure	Time	Humidity	# of samples & names
Binder	1 mm	60, 70, 85°C	150bar	3 weeks	$< 10\%$	3 (Q-60-HP-D)
Mixture	PA, SMA	60, 70, 85°C	150bar	3 weeks	$< 10\%$	6 (PA-60-HP-D)
Binder	1 mm	60, 70, 85°C	1bar	3 weeks	$> 90\%$, $< 10\%$	6 (Q-60-LP-W)
Mixture	PA, SMA	60, 70, 85°C	1bar	3 weeks	$> 90\%$	6 (PA-60-LP-W)

2020). A variant (VBA-Wet) included 75 g/m^3 humidity with similar oxidative gas concentrations (Khalighi et al., 2025b). The mastic samples were subjected to aging at the same temperature and pressure conditions, though additional details are provided in the table.

Table 3 presents the aging conditions for binder and mixture samples. For Q binder and Q mixtures (PA and SMA), LTA conditions included climate chamber treatment at different temperatures (60, 70, 85°C), and humidity levels ($< 10\%$ or $> 90\%$ RH), with thicknesses of 1 mm for 3 weeks. Furthermore, a custom-built oven was used to subject both binder and mixture samples to aging at 150 bar, allowing for studying the effects of extra-high pressure on thermo-oxidative ageing process.

Tables 2 and 3 presents all testing conditions for mastic samples and mixture samples, respectively, with corresponding binder samples as a comparison. The naming conventions for Table 2 are as follows: 'Q' represents the binder, 'W/W60k' denotes the mastic, and 'exW/exW60k' indicates the extracted binder. In Table 3, the naming system begins with either 'Q' for the original binder or 'PA/SMA' for the extracted binder from PA and SMA mixture samples, followed by the temperature. 'HP' and 'LP' signify high-pressure and low-pressure aging, respectively, while 'W' and 'D' refer to hygrothermal and thermo-oxidative aging. Examples of the naming format are provided in the last column of Tables 2 and 3.

4.4. Attenuated Total Reflectance-Fourier Transform Infrared (ATR-FTIR) spectroscopy

For most binder, mastic, and mixture samples, their chemical changes during aging were assessed using ATR-FTIR spectroscopy. Samples (~ 1 g) were heated to 110°C, stirred, and deposited on silicon foil (Mirwald et al., 2020; Mirwald et al., 2022) for analysis using a Nicolet iS5 Thermo Fisher Scientific instrument. Four spectra per aging state were generated in the 4000–400 cm^{-1} range. However, extracted binder samples aged at 150 bar were analysed using a Perkin Elmer Frontier model, with spectra recorded in the 4000–650 cm^{-1} range.

Table 4 lists the wavenumber ranges of main functional groups identified by the FTIR spectra for binder and extracted binder samples. Since the addition of filler changes the FTIR spectra significantly, Table 5 lists the wavenumber ranges of main functional groups identified by the FTIR spectra for mastic samples. Using the same wavenumber ranges as in Table 4 for the mastic samples would have excluded certain peaks, leading to a loss of relevant spectral information. Therefore, different vertical band limits were applied to accurately capture all significant data for the mastic samples.

Equations (1) was used to calculate the indices for each functional group with the tangential area under the curve and the vertical limits mentioned in Tables 4 and 5.

The computation of indices followed this equation:

$$index = A_x / A_{Total} \tag{1}$$

Table 4. Main functional groups of binder in FTIR spectra (Jing et al., 2021).

Area	Vertical band limit(cm^{-1})	Functional groups
A_{810}	710–734	Hydrocarbon chain, $(CH_2)_n$, C–H in isolated/two/four adjacent hydrogen aromatic rings or C–CH_2 rocking in alkyl side chains with more than four carbons
	734–783	
	783–833	
	833–912	
A_{1030}	984–1047	Oxygenated function-sulfoxide, S = O
A_{1200}	1100–1180	Tertiary alcohol C-C-O, C-O in carboxylic acid, C-C-C in diaryl ketones, C-N secondary amides, O = S = O in sulfone
	1280–1330	
A_{1376}	1350–1395	Branched aliphatic structures, CH_3
A_{1460}	1395–1525	Aliphatic structures, CH_3 and CH_2
A_{1600}	1535–1670	Aromatic structure, C = C
A_{1700}	1660–1750	Oxygenated function-carbonyl, C = O
A_{2953}	2820–2880	Aliphatic structures, Symmetric, Asymmetric stretching, CH
	2880–2990	
A_{3400}	3100–3600	Hydroxyl stretching, OH, NH
A_{Total} = A 810 + A 1030 + A 1200 + A 1376 +A 1460 + A 1600 +A 1700 +A 2953+ A3400		

Table 5. Main functional groups of mastic in FTIR spectra.

Area	Vertical band limit(cm^{-1})	Functional groups
A_{810}	680–734	Hydrocarbon chain, $(CH_2)_n$, C–H in isolated/two/four adjacent hydrogen aromatic rings or C–CH_2 rocking in alkyl side chains with more than four carbons, Thiols, Out-of-plane and in-plane bending of carbonate (CO_3^{2-})
	734–783	
	783–833	
	833–912	
A_{1030}	930–1120	Oxygenated-sulfoxide, S = O, sulfur compounds, silicate
A_{1376}	1350–1395	Branched aliphatic structures, CH_3
A_{1460}	1395–1525	Aliphatic structures, CH_3 and CH_2, asymmetric stretching of carbonate (CO_3^{2-})
A_{1600}	1550–1660	Aromatic structure, C = C
A_{1700}	1660–1735	Oxygenated function-carbonyl, C = O
A_{2953}	2820–2880	Aliphatic structures, Symmetric, Asymmetric stretching, CH
	2880–2990	
A_{3400}	3100–3700	Hydroxyl stretching, OH, NH
A_{Total} = A 810 + A 1030 + A 1376 +A 1460 + A 1600 +A 1700 +A 2953+ A3400		

The symbol A_x denotes the tangential peak area under the curve within specific ranges outlined in Tables 4 and 5.

One of the primary objectives of this study is to assess if FTIR spectra can be utilised to effectively characterise and compare aging behaviour of bituminous materials at multiple scales. To improve the accuracy of the information extracted from FTIR, a series of preprocessing procedures is required. For all spectra, pre-processing included an 8-point baseline correction (Table 5S) and normalisation of absorbance values using the NMO method (Khalighi et al., 2024c; Porot et al., 2023). Additionally, the advanced ATR correction algorithm implemented in the OMNIC™ 6.2 software for Thermo Scientific Nicolet™ FT-IR spectrometers was utilised in this study. To apply this advanced ATR correction, four inputs are required: the refractive index of the sample, the refractive index of the ATR crystal, the angle of incidence, and the number of bounces. Among these parameters, three are determined by the accessory itself: the refractive index of the internal reflection element (IRE) is dictated by the crystal material, while the angle of incidence and the number of bounces are defined by the accessory's design. The refractive index of the sample material typically hovers around 1.5 for most organic substances; using this value generally yields optimal correction performance according to manufacturer.

In a transmission experiment, the pathlength is defined by the sample thickness and remains constant across the spectrum. However, in ATR, the depth of infrared beam penetration into the sample

varies with wavelength, as described by Equation (2):

$$d_p = \frac{\lambda}{2\pi n_1 \sqrt{sin^2 \emptyset - (n_2/n_1)^2}} \tag{2}$$

where dp, λ, $\emptyset$, n1, and n2 are the penetration depth, wavelength, incident angle, ATR crystal refractive index, and sample refractive index, respectively. The relative intensity of bands in an ATR spectrum increases with wavelength. Many FTIR software packages apply an ATR correction that approximates the relative band intensities expected in a transmission experiment by applying a linear correction factor. However, because the refractive index of the sample (n_2) changes sharply near absorption bands, the wavelength dependence of dp is further modified according to $\sin^2\theta - (n_2/n_1)^{-1/2}$.

Another key characteristic of ATR spectra is the shift of absorption bands to lower frequencies. Since the refractive index of the sample influences dp, instead of α, the term $n_2 dp\alpha$ determines the exact band positions. Due to anomalous dispersion, this effect systematically shifts absorption bands to lower frequencies, particularly for strong absorptions.

Furthermore, to assess whether ATR correction in the pre-processing step influences the qualitative analysis of FTIR spectra, indices were computed for both corrected and uncorrected spectra. For conciseness, only the indices from the corrected spectra are presented in the main text, while those from the uncorrected spectra are included in the supplementary information (Figure 4S and 5S). A comparison of these two sets of indices reveals that the trends in changes for various functional groups remain consistent; only the absolute values differ. This outcome was anticipated since normalised values were employed in both analyses to mitigate the impact of refractive index discrepancies. Given that the trends align across both analyses, the following discussion will focus on the ATR-corrected values.

4.5. Principle component analysis (PCA)

PCA is a key technique for converting datasets with numerous variables into uncorrelated components, facilitating dimensionality reduction. The scores for the target samples are computed using the equation $\mathbf{Y} = \mathbf{X} \times \mathbf{W}$, where $\mathbf{X}$ represents the dataset comprising m samples (organised into l categories) and n variables. The matrix $\mathbf{W}$, an n × p loading matrix, indicates the number of selected principal components, while $\mathbf{Y}$ forms an m × p score matrix that describes the projection of $\mathbf{X}$ into a p-dimensional feature space. To derive $\mathbf{W}$, the eigenvectors and eigenvalues of the covariance matrix of the variables within the spectral dataset are calculated. The eigenvalues are then arranged in descending order, and the top p eigenvectors corresponding to the largest eigenvalues are selected to construct W. Furthermore, PCA loadings are analysed to identify significant regions for cluster formation (Ma et al., 2023b).

The dataset utilised for PCA analysis comprised FTIR results, including all indices detailed in Tables 4 and 5, with four peaks within the range of 680–912 cm^{-1} treated as distinct indices. Furthermore, the entire FTIR spectra were also employed for analysis and comparison against the indices.

4.6. Pairwise Euclidean distance

Pairwise Euclidean distance refers to the computation of distances between pairs of points in a multi-dimensional space, specifically measuring the straight-line distance between each pair using the Euclidean distance formula (Domazet-Lošo & Haubold, 2009). To determine the proximity of laboratory conditioning for mixture samples to that of binder samples, pairwise distances were calculated based on the principal components. The Euclidean distance was employed to quantify the straight-line distance between two points in the selected high-dimensional space, calculated as follows in Equation (3):

$$\text{Euclidean distance} = \sqrt{((p_1 - q_1)^2 + (p_2 - q_2)^2 + \ldots + (p_d - q_d)^2} \tag{3}$$

where (p_1,p_2,… ,p_d) and (q_1,q_2,… ,q_d) represent the coordinates of the two points.

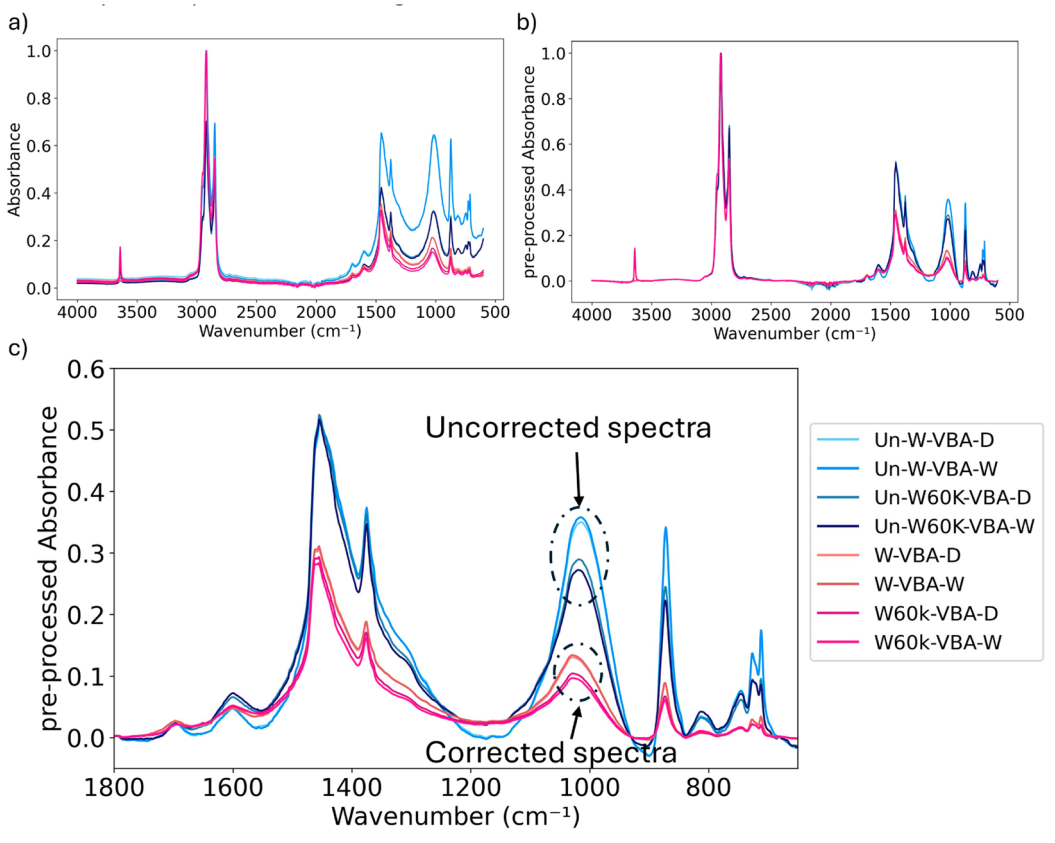

Figure 1. Comparison between uncorrected and advanced ATR corrected spectra: (a) raw FTIR spectra, (b) baseline-corrected and normalised spectra, and (c) the spectra in the range of 650-1800cm^{-1} with baseline and normalisation correction. 'Un' in the legend refers to the uncorrected spectra.

In this context, a larger Euclidean distance between two points signifies a greater dissimilarity between the conditioning effects on the samples, indicating that the conditioning processes may be yielding different material responses. Conversely, a smaller Euclidean distance suggests a closer similarity, implying that the laboratory conditioning is comparable across the sample types.

5. Results and discussion

5.1. FTIR pre-processing

Figure 1a presents the raw FTIR spectra with and without advanced ATR correction (AAC) for mastic samples. Notably, the differences between spectra are more pronounced for the uncorrected ATR-FTIR spectra. The advanced ATR correction effectively mitigates the distortion of relative peak intensities, especially at lower wavenumbers, thereby facilitating a clearer visual comparison of the mastic and binder spectra.

FTIR data also exhibited varying baselines and differences in the overall intensity of the spectra due to samples, instrument, or experimental conditions, necessitating the application of baseline correction and normalisation techniques (Khalighi et al., 2024c). As shown in Figure 1 b and c, spectra after three pre-processing steps show increased comparability of the results. In conclusion, the integration of ATR correction, baseline correction, and normalisation as pre-processing steps in FTIR analysis is recommended to enhance spectral quality and facilitate more accurate sample comparisons.

However, it is important to acknowledge that this study assumed identical refractive indices for both binders and mastics. In reality, binders and mastics may possess different refractive indices, which can affect the penetration depth of the IR beam in ATR mode. Future investigations should address these variations to enable more accurate comparisons of absorbance intensities and peak positions.

Moreover, the slight tilting of the aliphatic peak around 1450 cm^{-1} observed in Figure 1 is likely due to the ATR correction applied during spectral pre-treatment. ATR correction compensates for wavelength-dependent penetration depth, which can occasionally introduce minor alterations, particularly in regions with strong absorption bands. However, this distortion does not significantly affect the proposed methodology. The primary purpose of the pre-treatment is to ensure comparability between spectra and to correct for variations arising from ATR sampling depth and baseline inconsistencies. Since the aging analysis is based on relative peak intensities and overall spectral trends rather than absolute peak shapes, the methodological conclusions remain robust.

5.2. Comparison between mastic and binder samples

Figure 2 presents the raw and pre-processed FTIR spectra for both mastic and mastic-extracted binder. While both mastic and binder samples display similar peaks across most regions, their absorbance values differ significantly. For instance, the presence of fillers in the mastic samples leads to increased absorbance, particularly evident in the long-chain and sulfoxide peaks. In the 1100-1350 cm^{-1} region, the spectral shapes diverge considerably, likely due to the strong adjacent sulfoxide peak and the presence of fillers. Notably, no new strong peaks emerge in the mastic samples within these regions. Additionally, W60k fillers introduce a minor peak in the hydroxyl group region (3600-3700 cm^{-1}) because of hydroxyl groups present in $Ca(OH)_2$.

To further compare the aging behaviour in binders and mastics, along with the influence of different fillers (hydrated lime vs limestone) and the behaviour of extracted binders, FTIR indices were calculated for all peaks outlined in Table 5, and results were plotted in Figures 3 and 4. By examining changes in chemical indices such as carbonyl, sulfoxide, hydroxyl, aromatic, and aliphatic contents, we highlighted how fillers and environmental conditions like ROS (VBA-DRY) and humidity (VBA-WET) significantly influence aging behaviour.

5.2.1. Effect of filler type on aging of mastic samples

The comparison between W mastic (limestone filler) and W60k mastic (hydrated lime filler) underscores the distinct roles fillers play in aging processes. W60k mastic exhibited lower carbonyl (Figure 3a) and aliphatic indices (Figure 3e) under VBA-WET aging than W mastic, highlighting hydrated lime's protective effect against oxidative aging. Hydrated lime's alkaline properties likely neutralise acidic oxidation products, slowing down the aging process, while limestone appears to accelerate oxidative degradation. The sulfoxide index (Figure 3b), however, was higher in W60k mastic, particularly under wet conditions, suggesting that while hydrated lime reduces carbonyl formation, it may promote sulfur oxidation more than limestone.

In terms of the hydroxyl index (Figure 3c), W60k mastic exhibited significantly higher values compared to W mastic, attributable to the intrinsic hydroxyl groups present in hydrated lime. The aromatic index (Figure 3d) and long-chain indices (Figure 4a-d) showed inconsistent trends across both samples, reflecting the complex interaction between filler type and aging. Overall, hydrated lime fillers, especially under humid conditions, demonstrated better oxidative resistance, selectively inhibiting certain oxidation pathways such as carbonyl formation while being less effective against sulfur-containing compounds.

5.2.2. Comparing aging between binders and mastics

For most binder and mastic samples, ageing led to increases in FTIR indices, particularly the carbonyl (Figure 3a), sulfoxide (Figure 3b), and hydroxyl indices (Figure 3c). These increases reflect the oxidative aging processes driven by reactive oxygen species (ROS) in dry and humid environments. The

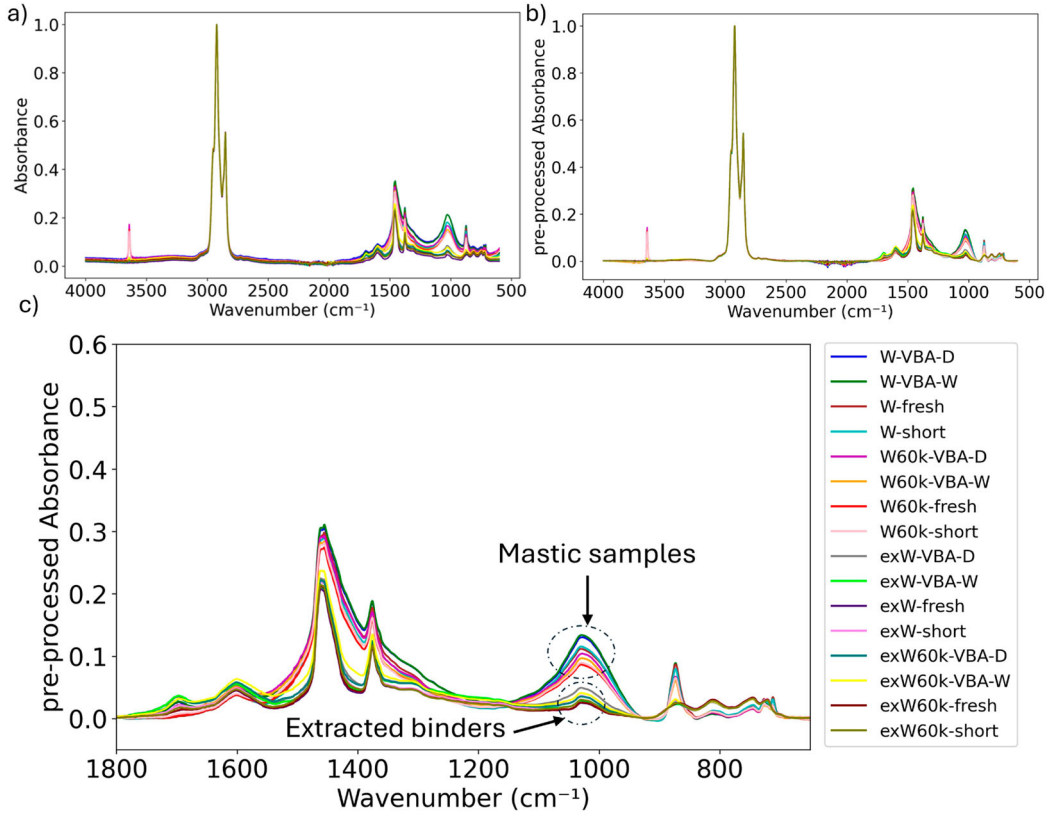

Figure 2. FTIR spectra (a) after ACC preprocessing, (b) after ACC, baseline, and normalisation preprocessing, and (c) in the range of 650–1800cm^{-1} with ACC, baseline, and normalisation corrections for fresh, short-term aged, and long-term aged mastic and mastic-extracted binder samples.

addition of humidity in the ageing process of bituminous binders accelerates ageing as indicated by the generation of more polar groups. However, this effect varies significantly when fillers are present or under mixture conditions. For most samples, the aging was more pronounced in the presence of humidity (VBA-WET) compared to the dry condition, as revealed by the carbonyl and sulfoxide indices, indicating that humidity accelerated the oxidation reactions.

Notably, the aliphatic index (Figure 3e) decreased under both dry and wet VBA aging conditions, indicating a breakdown of aliphatic structures in both binders and mastics. The aromatic index (Figure 3d) showed inconsistent behaviour between binder and mastics, likely due to the interference of overlapping peaks caused by the presence of fillers. Meanwhile, long-chain indices (Figure 4a-d) demonstrated complex changes at different ageing conditions, which also differs across different binder and mastic sample types, further reflecting the intricate effects of fillers on the binder aging process.

5.2.3. Comparing aging between binders and mastic-extracted binders

The aging of mastic-extracted binders is influenced by both fillers and the extraction process, though the latter plays a primary role. Extracted binders showed higher carbonyl (Figure 3a) and sulfoxide indices (Figure 3b) after aging under VBA-DRY conditions compared to the original binder samples, likely due to secondary chemical reactions during extraction. However, Under VBA-WET conditions, extracted binders from W60k mastic (with hydrated lime) exhibited lower carbonyl index values than original binders, highlighting the protective role of hydrated lime against carbonyl formation. This

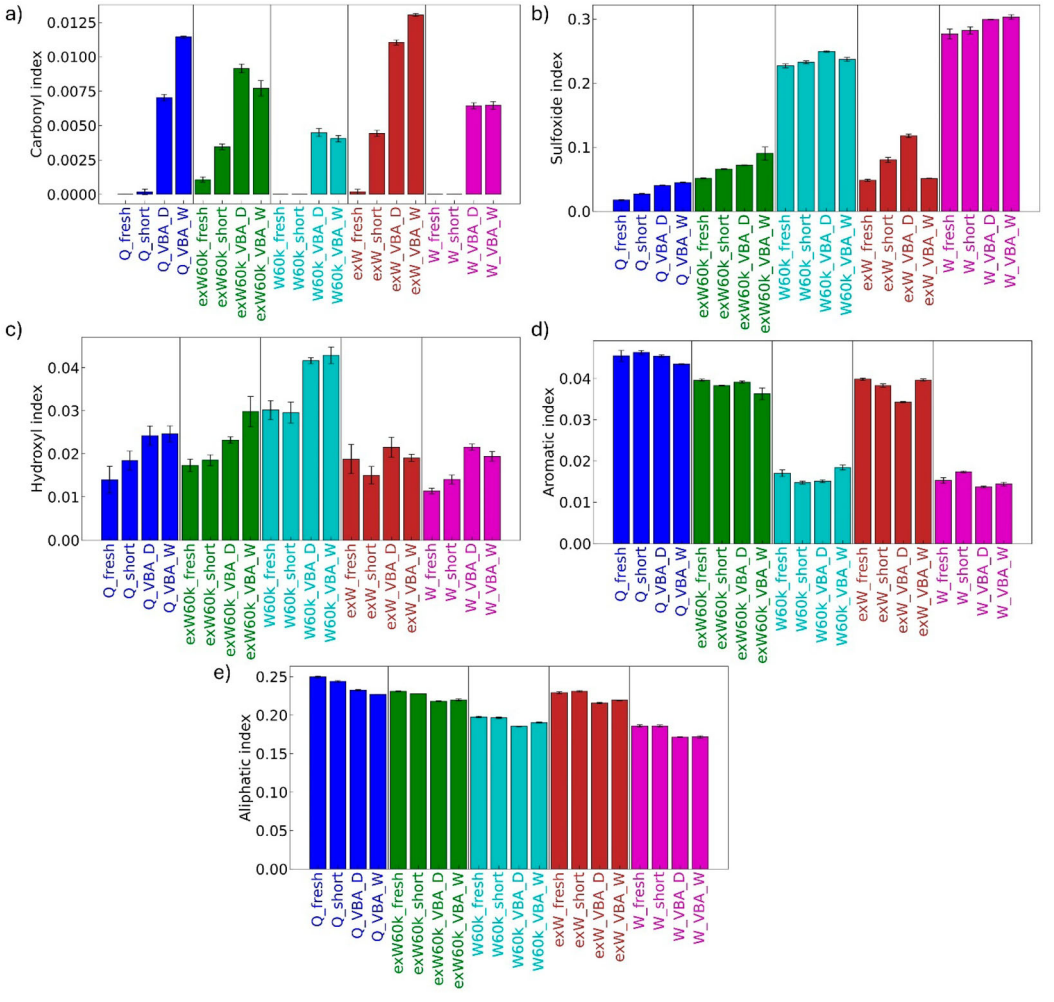

Figure 3. FTIR indices of (a) carbonyl, (b) sulfoxide, (c) sulfone, (d) hydroxyl, (e) aromatic, and (f) aliphatic functional groups. Results are presented for all binders, mastics, and binders extracted from mastics samples at fresh, short-term, and long-term (VBA-wet and VBA-DRY) aging states.

can be attributed to the higher Rigden voids (RV) of hydrated lime (RV = 47%) compared to limestone filler (RV = 38%), which allows for greater bitumen fixation and reduces the amount of binder exposed to oxidative aging mechanisms. In contrast, the extracted binder from W mastic (limestone) showed higher carbonyl and sulfoxide indices under VBA-WET, suggesting that limestone accelerates oxidation more than hydrated lime in humid conditions. The low RV of limestone filler (RV = 38%) results in less bitumen being physically immobilised, leaving more binder vulnerable to oxidative aging. These findings indicate that RV plays a crucial role in the aging resistance of mastics, further reinforcing the anti-aging benefits of hydrated lime in asphalt mixtures.

The hydroxyl index (Figure 3c) of the extracted binder from the long-term aged W60k mastic was found to be comparable to that of the original long-term aged binder. In contrast, the extracted binder from the long-term aged W mastic exhibited significantly lower hydroxyl values than those of the original long-term aged binder. This suggests that hydrated lime helps preserve hydroxyl functionality, while limestone is less effective in this regard. The aliphatic index (Figure 3e) decreased more significantly in extracted binders, particularly after LTA under VBA-WET conditions, implying enhanced breakdown of aliphatic structures during extraction.

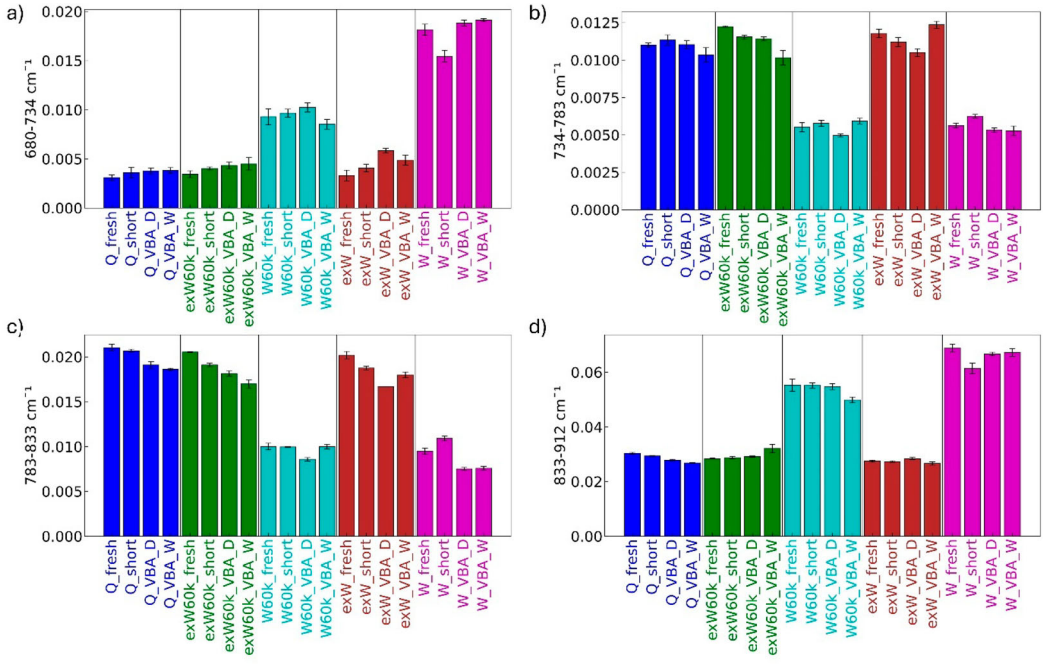

Figure 4. FTIR indices of peaks at regions of (a) 680-734 cm^{-1}, (b) 734-783 cm^{-1}, (c) 783-833 cm^{-1}, and (d) 833-912 cm^{-1}. Results are presented for all binders, mastics, and binders extracted from mastics samples at fresh, short-term, and long-term (VBA-wet and VBA-DRY) aging states.

Further research is needed to gain a deeper understanding of the effects of extraction on aging of bituminous binders and its underlying mechanisms, particularly to explain the variations observed between fresh and aged samples.

5.2.4. Comparing aging among binders, mastics, and mastic-extracted binders

Mastic samples consistently displayed lower carbonyl (Figure 3a) and aliphatic indices (Figure 3e) and higher sulfoxide index compared to both original and extracted binders. This is likely due to fillers either masking functional groups or broadening spectral peaks, making them less detectable. Conversely, mastics showed higher sulfoxide indices (Figure 3b), which may be attributed to sulfur-containing or silicate groups in hydrated lime and limestone fillers. These disparities in FTIR indices indicate that direct comparisons between binders and mastics are challenging, as fillers significantly alter the spectral behaviour.

Due to complex interactions between the binder, fillers, and extraction process, the aromatic (Figure 3d), aliphatic index (Figure 3e) and long-chain indices (Figure 4a-d) were less reliable for direct comparisons.

As a summary, the oxidative aging mechanisms of binders and mastics depend on the chemical reaction processes driven by reactive oxygen species (ROS) and humidity and the nature of the fillers. For binders, the interaction with ROS under wet conditions (VBA-WET) accelerates the formation of carbonyl and sulfoxide compounds compared to the dry one. while by analysis extracted binders, fillers like hydrated lime act as alkaline agents that neutralise acidic oxidation products, thereby inhibiting oxidative reactions. The selective anti-aging effect of hydrated lime is evident, as it effectively mitigates carbonyl formation but promotes sulfur oxidation. The extraction process introduces complexity due to potential secondary chemical reactions, which further increases oxidation in extracted binders. Further research is necessary to confirm this observation.

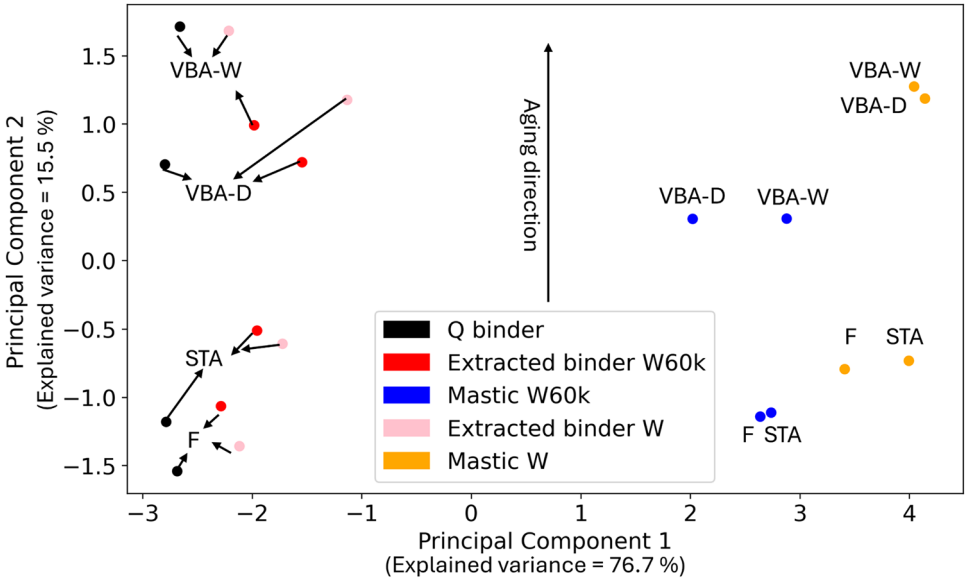

Figure 5. PCA plot based on FTIR indices data for fresh, short-term aged, and VBA long-term aged samples including Q binder, mastic samples and extracted binder from mastic samples.

Different factors, including humidity, filler type, and extraction, influence the aging process at various scales, from binder to mastic samples. Active fillers like hydrated lime can protect the binder from oxidative aging, especially under wet conditions, but their removal during extraction can lead to enhanced aging in the extracted binders. Thus, the presence and type of filler are crucial in controlling the aging behaviour at both the binder and mastic levels.

5.2.5. PCA analysis of binders and mastics

The complex variations of individual FTIR indices across different binder and mastic samples and aging conditions necessitate a further comparison of binders and mastics combining all FTIR indices. To achieve this, PCA was conducted using all binder and mastic samples. The first two principal components account for over 90% of the variance (Figure 2S), therefore, a two-dimensional plot of PC1 versus PC2 is presented in Figure 5. As shown in the plot, a clear distinction is observed between original binders, extracted binders, and mastic samples along PC1, highlighting the distinct chemical differences caused by the extraction process and the presence of filler, regardless of ageing states.

PC2 shows the trends in aging, where higher PC2 values correspond to more aging. For both original and extracted binders, a larger difference in the PC2 values is observed between VBA-WET and VBA-DRY conditions. In contrast, mastic samples show more similar PC2 values for both conditions, suggesting that the presence of filler masks the aging-related chemical changes characterised by the FTIR indices. Furthermore, for both mastics and extracted binders, samples containing hydrated lime (W60k) consistently occupy lower positions on the PC2 axis compared to those with limestone (W), indicating less aging in samples containing hydrated lime.

Figure 6 shows the loadings of features contributing to PC1 and PC2. PC1 is mainly influenced by FTIR indices in the regions of 680–734 cm^{-1} and 783–838 cm^{-1}, as well as the carbonyl region (1660–1735cm^{-1}) and the sulfoxide region (930–1120 cm^{-1}). Interestingly, while raw FTIR spectra displayed clear differences in the long-chain and sulfoxide regions between mastics and binders, changes in the carbonyl region were less apparent. However, the combination of FTIR index calculations and PCA analysis helped reveal the significance of the carbonyl region. PC2, which captures aging direction,

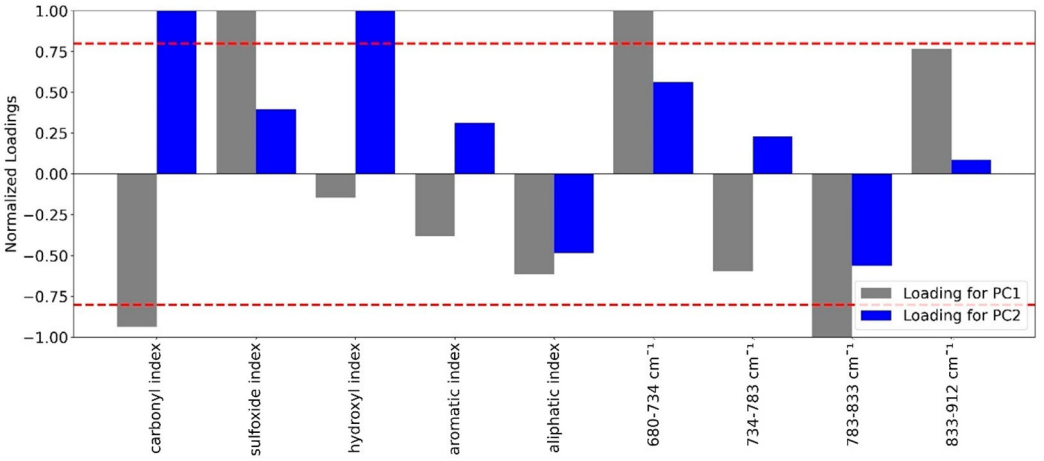

Figure 6. Loading of all features (fresh, short-term aged, and VBA long-term aged samples including Q binder, mastic samples and extracted binder from mastic samples) on PC1 and PC2. A threshold of ± 0.80 was applied to determine the significance of these loadings.

is heavily influenced by indices from the carbonyl and hydroxyl regions, emphasising their roles in aging processes.

5.3. Comparison between mixture and binder samples

Figure 7 presents the FTIR spectra of both binder samples and binder extracted from mixture samples. For clarity, the term 'mixture sample' will refer to the binder extracted from the mixture samples in the subsequent sections. Based on Figure 6, the binder and mixture samples show similar spectral peaks across various regions, except in the 1100-1350 cm^{-1} region, where new peaks are observed in the mixture samples (Figure 6 b).

5.3.1. Effects of aging on binder and mixture samples

To further analyse the ageing behaviour of binder and mixture samples, the FTIR indices for specific peaks listed in Table 5 were calculated, with results shown in Figures 8 and 9. FTIR indices of binder and mixture samples show that all indices change with the same trend with varying ageing conditions at both scales. This observation suggests that the aging mechanisms affecting the binder are consistent with those in the mixtures and that the chemical changes observed in the binder are reflective of the changes occurring within the mixture. This may also suggest that binder-level tests can provide insight into the aging processes within mixtures. To further explore this relationship, the following contents will evaluate the effect of each aging factor—temperature, pressure, and humidity—on both binder and mixture samples.

The influence of temperature on the aging indices is observed consistently across binder and mixture samples. As shown in Figure 8a, the carbonyl index increases with rising temperatures for both binder and mixture samples at all pressure levels, highlighting the strong oxidative effects of heat on these materials. PA mixtures show a more pronounced increase in the carbonyl index at lower temperatures and pressures, whereas SMA mixtures exhibit higher aging at 85°C and 150 bar, suggesting temperature and sample type play a key role in oxidative aging. Similarly, in Figure 8b, the sulfoxide index increases with temperature in binder samples aged at lower pressures. However, no clear temperature dependence is seen for binder samples aged at 150 bar, while mixture samples exhibit either a reduction or no significant change in the sulfoxide index with temperature, possibly due to the degradation of sulfoxide molecules at higher temperatures. For the sulfone index (Figure 8c), both

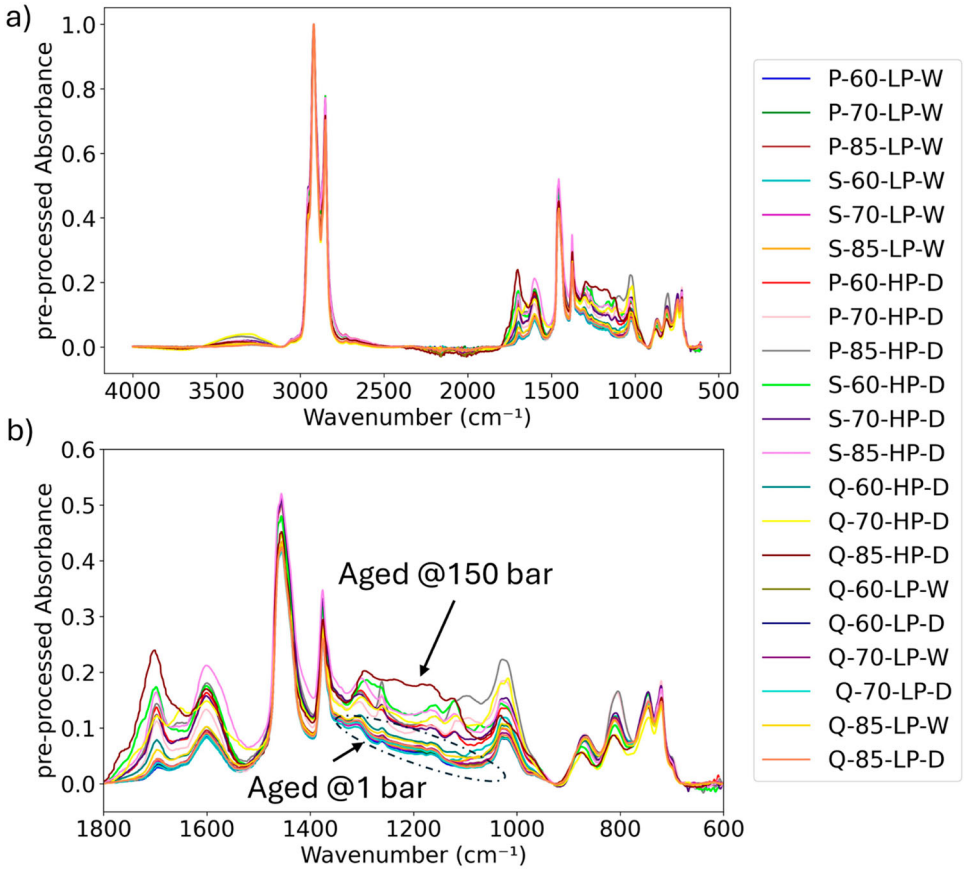

Figure 7. FTIR spectra of binder and mixture samples (a) after pre-processing and (b) at the range of 650-1800cm^{-1}.

binder and mixture samples show a clear increase with rising temperatures at all pressure levels, indicating its temperature sensitivity. In contrast, Figure 8d reveals no consistent trend for the hydroxyl index with temperature, while the aromatic index (Figure 8e) increases with temperature across all samples. Lastly, the aliphatic index (Figure 8f) shows a slight decrease with increasing temperatures, indicating temperature-induced degradation of aliphatic compounds. Similarly, the long-chain index in Figure 9 decreases with increasing temperature in both binder and mixture samples, more so at higher pressures.

Pressure significantly influences the aging behaviour of both binder and mixture samples. In Figure 8a, the carbonyl index is markedly higher in samples aged at 150 bar compared to those aged at 1 bar, demonstrating that high pressure intensifies aging, especially in SMA mixtures at higher temperatures. The sulfoxide index (Figure 8b) also increases with pressure, although this trend is less pronounced than that for the carbonyl index. Notably, at 150 bar, the sulfoxide index decreases or remains constant with increasing temperature, suggesting that under harsher aging conditions, degradation of sulfoxide molecules outpaces their formation. The sulfone index (Figure 8c) exhibits a stronger increase with pressure than temperature, with samples aged at 150 bar consistently showing higher values than those aged at 1 bar. Conversely, the hydroxyl index (Figure 8d) shows higher values at 150 bar but lacks a clear trend with pressure. In Figure 7e, the aromatic index increases more significantly at 150 bar, indicating that higher pressures enhance aromatic compound oxidation. The aliphatic index (Figure 8f), however, decreases more rapidly at higher pressures, indicating a pressure-induced

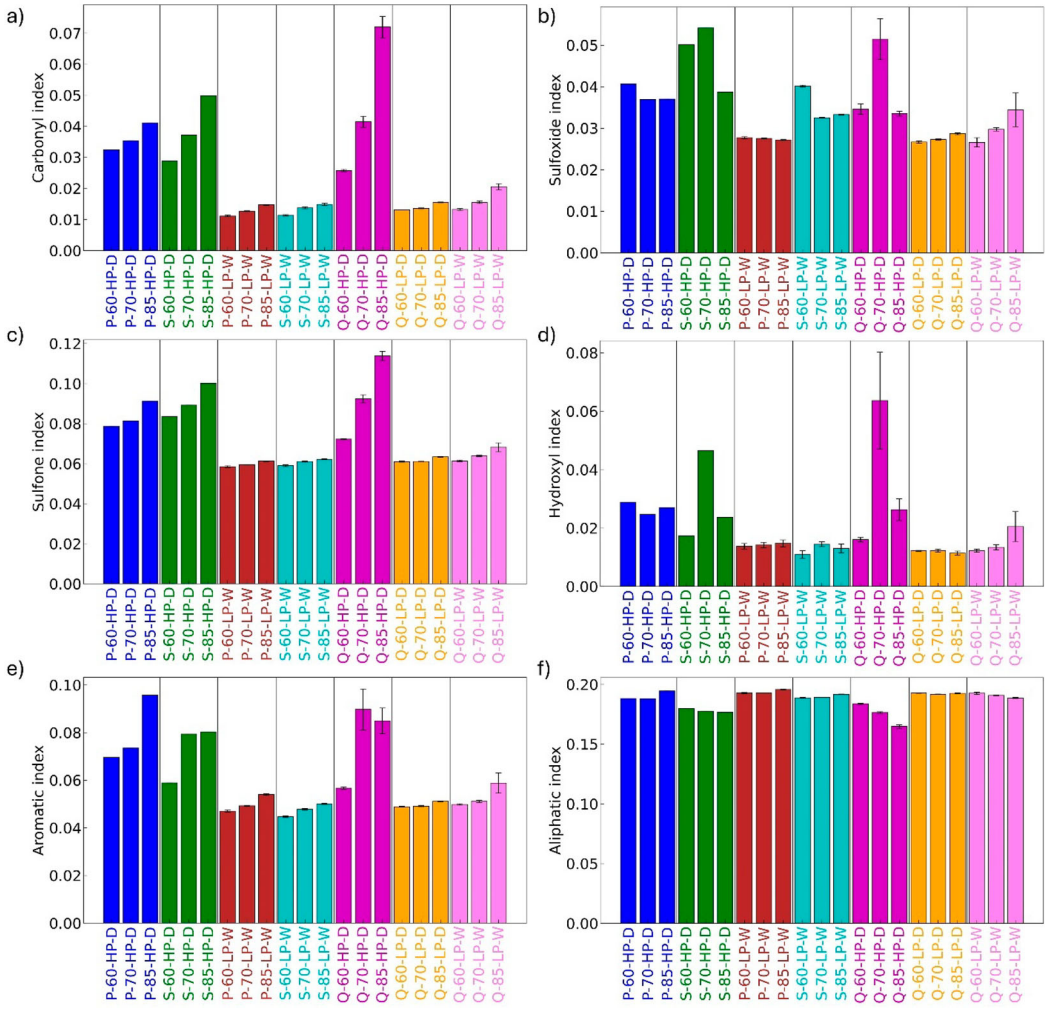

Figure 8. (a) carbonyl index, (b) sulfoxide index, (c) sulfone index, (d) hydroxyl index, (e) aromatic index, and (f) aliphatic index of binder (Q) and mixture (P and S) samples at different temperatures of 60, 70, and 85 °C and pressures of 1 bar (LP) and 150 bar (HP). W and D represent the humidity levels of $<$ 10% and $>$ 90% relative humidity during aging, respectively.

degradation of aliphatic structures. The long-chain index (Figure 9) also exhibits a steeper decrease at higher pressures, aligning with the observed trends for the aromatic and aliphatic indices.

Humidity also plays an important role in the aging process, particularly for binder samples. As observed in Figure 8a, humidity further increases the carbonyl index in binder samples, at higher temperatures, indicating that moisture accelerates oxidation at elevated temperatures. A similar trend is seen for the sulfoxide index (Figure 8b), where humidity increases its value in binder samples, particularly at elevated temperatures. For the sulfone index (Figure 8c), humidity enhances its increase in binder samples, again more so at higher temperatures. In contrast, humidity has little effect on the hydroxyl index (Figure 8d), with no significant changes observed. Humidity also increases the aromatic index in binder samples (Figure 8e), particularly at elevated temperatures, but leads to a slight decrease in the aliphatic index (Figure 8f). This suggests that humidity may promote the formation of aromatic compounds while contributing to the breakdown of aliphatic structures. The long-chain index (Figure 9) decreases with humidity in binder samples, especially at higher temperatures, suggesting that moisture accelerates the breakdown of longer alkyl chains.

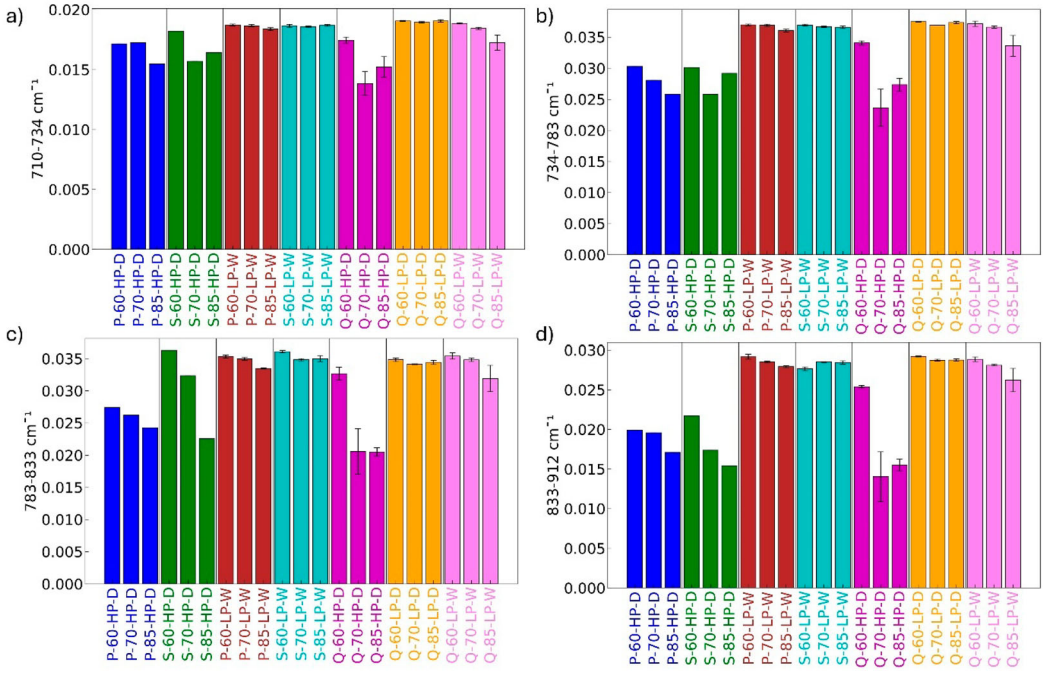

Figure 9. FTIR indices of peaks in the ranges of (a) 710-734 cm^{-1}, (b) 734-783 cm^{-1}, (c) 783-833 cm^{-1}, (d) 833-912 cm^{-1} for binder (Q) and mixture (P and S) samples at different temperatures of 60, 70, and 85 °C and pressures of 1 bar (LP) and 150 bar (HP). W and D represent the humidity levels of $< 10\%$ and $> 90\%$ relative humidity during aging, respectively.

5.3.2. Comparison of PA and SMA mixtures

PA and SMA mixtures exhibit distinct aging behaviours due to their structural differences. PA mixtures, with their higher air void content, show more pronounced aging compared to SMA at lower temperatures and pressures, as indicated by the higher carbonyl indices in Figure 8a. However, at higher temperatures and pressures, SMA mixtures exhibit greater aging, as seen in the carbonyl and sulfone indices (Figure 8a and Figure 8c). This finding is counterintuitive, as PA, with its higher porosity and greater exposed surface area, would be expected to undergo more oxidative aging. While potential test errors cannot be entirely ruled out, further research with additional replicates of PA and SMA samples is necessary to confirm this observation. The sulfoxide index (Figure 8b) shows a reduction or no change with increasing temperature in PA mixtures, indicating sulfoxide degradation under harsh aging conditions. Interestingly, both PA and SMA samples exhibit similar hydroxyl index values at lower pressures (Figure 8d), while at 150 bar, the variations are inconsistent, making it difficult to directly compare the aging levels of the two mixtures based on this index. In terms of the aromatic index (Figure 8e), PA samples show higher values across all conditions, indicating more aromatic group in these mixtures compared to SMA. Finally, the long-chain index (Figure 9) shows more pronounced aging in PA mixtures at higher pressures, aligning with the trends observed in the aromatic index but contrasting with those of the sulfoxide index.

5.3.3. PCA analysis of binders and mixtures

As discussed in the previous section, the changes in FTIR indices can be complex, depending on the FTIR index, sample type, and aging conditions. Therefore, it is advantageous to employ methods that consider all indices collectively, providing a comprehensive perspective on aging across different samples. PCA is one such method that aids in identifying the main contributors to aging, which is crucial for both classification and regression analysis. In this study, PCA was performed on both binder and mixture samples, using their chemical properties, namely FTIR indices, as input variables. The first two

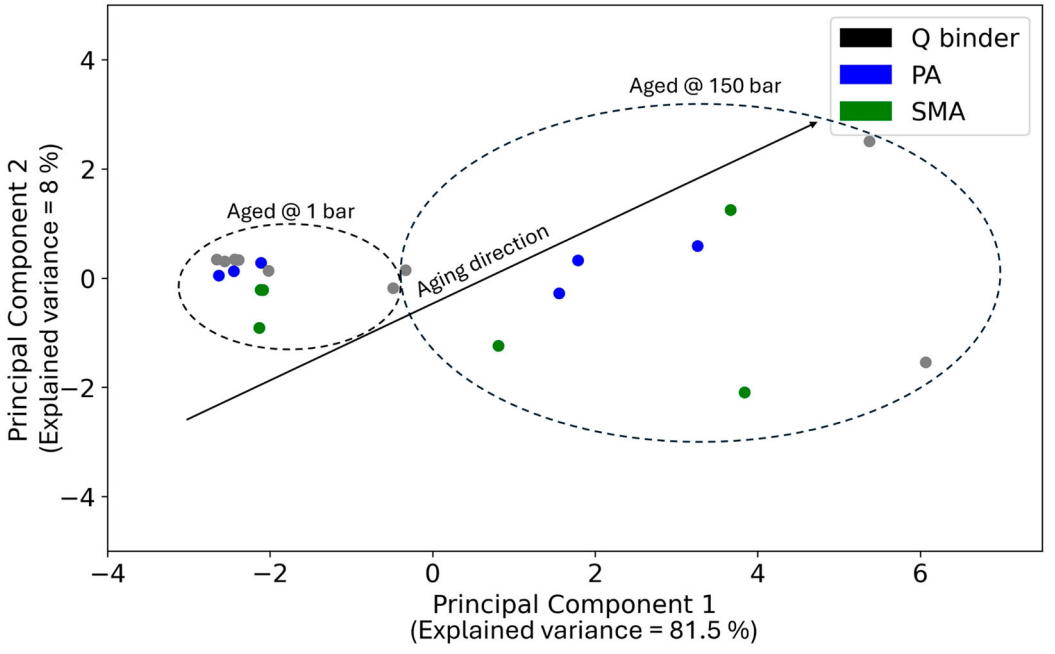

Figure 10. PCA plot based on FTIR indices data for long-term aged samples including Q binder, PA and SMA mixtures.

principal components (PCs) account for over 80% of the variance in the data, based on the explained variance (Figure 3S). Thus, a two-dimensional plot of PC1 versus PC2 (Figure 10) effectively captures the majority of the data's variability.

As shown in Figure 10, there is a clear separation between samples aged at 1 bar and those aged at 150 bar, for both binder and mixture samples. This indicates that PC1 clearly shows the effects of pressure on aging. Furthermore, the direction of aging due to temperature trends towards the top-right quadrant of the PCA plot, suggesting that aging increases with both principal components.

PCA loadings, which represent the contribution of the original variables to the principal components, were normalised within a range of -1 to $+1$. A threshold of ± 0.8 was set, with variables exceeding this threshold deemed significant. The sign of the loading indicates whether the variable is positively or negatively correlated with the principal component.

Figure 11 displays the loadings for both PC1 and PC2. For PC1, key contributors include FTIR indices in the regions of 783-912 cm^{-1} (C–H bending vibrations in aromatic rings), 1535-1670 cm^{-1} (aromatic structure), and the sulfoxide group in the 984-1047 cm^{-1} range. These regions align with the fingerprint area in the FTIR spectra, which also revealed pressure effects, highlighting the role of pressure in aging. For PC2, the loadings emphasise the effect of temperature on aging, with key contributors including FTIR indices in the 783–833 cm^{-1} range (C–H in isolated aromatic rings), the sulfoxide group in the 984-1047 cm^{-1} region, and the 3100-3600 cm^{-1} range corresponding to hydroxyl functional groups. This indicates that long-chain regions, sulfoxide, aromatic, and hydroxyl groups are critical in determining the effects of both pressure and temperature on the aging of binder and extracted binder samples.

5.4. Can aging at binder level provide insights into the aging mechanisms at the mastic and mixture scale?

Based on the above observations, FTIR analysis at the binder level may not fully capture the aging processes observed in mastics and mixtures, due to several factors. One of the primary reasons is the

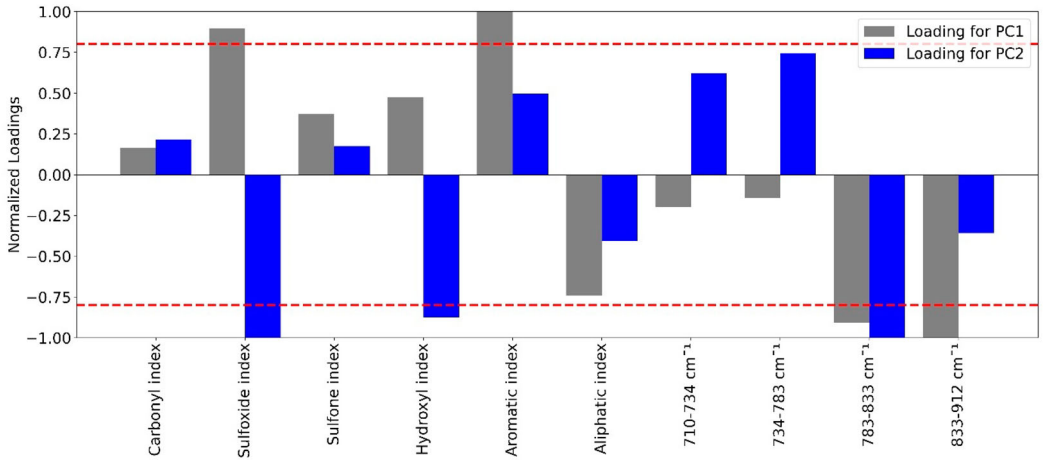

Figure 11. Loading of all features for PC1 and PC2 (obtained from PCA analysis using FTIR indices for long-term aged samples including Q binder, PA and SMA mixtures). A threshold of ± 0.80 was applied to determine the significance of these loadings.

variability in FTIR indices between binders and mastics due to the presence of filler. Fillers reveal peaks in similar spectral regions as binders, especially those changing with ageing such as carbonyl and sulfoxide indices, complicating the interpretation of key chemical changes in mastics. Furthermore, the presence of fillers in mastics, such as limestone and hydrated lime, significantly affects sample viscosity, which may also influence aging processes. The increased viscosity of mastics, resulting from filler content, could reduce the diffusion rates of oxygen and other reactive species, potentially slowing down oxidation kinetics and altering oxidation pathways compared to binders. These effects add complexity to the analysis of chemical changes in mastics. For instance, hydrated lime in W60k mastics has been shown to reduce carbonyl formation under wet aging conditions, a protective effect not observed in binders. This interaction introduces additional complexity, making it challenging to generalise aging behaviour based on binder studies alone.

At the mixture level, the presence of aggregates, along with the type and morphology of the mixture, such as air void content and connectivity, significantly impacts aging, leading to varied ageing rate and oxidative reaction procedures. These factors introduce additional variability that cannot be captured by studying binder-level aging alone, emphasising the need to investigate aging processes across multiple scales to understand the behaviour of the entire asphalt system.

Moreover, extracted binders, particularly those subjected to wet aging, show higher carbonyl and sulfoxide content compared to original binders, indicating that the extraction process itself may induce additional oxidative. This highlights the limitations of comparing ageing at different scales using binders extracted from mastic and mixture samples.

Although aging at the binder level cannot fully represent the exact aging processes observed in mastic and mixture levels, quantifying how different the aging processes are between binder and mastic, or mixture levels helps to assess the applicability of binder-level studies for predicting mastic and mixture aging behaviour. To this end, a Euclidean distance matrix was calculated to quantify how far apart the aging behaviours of different samples (e.g. binder vs. mastic/mixture) are in the PCA space.

Due to the presence of filler, using FTIR spectra to interpret the ageing mechanisms in mastics and to compare the ageing behaviour in binders and mastics remain challenging. Therefore, comparisons in this study will focus on binder samples and binder extracted from mastic and mixture samples to provide more accurate insights.

Figure 12 presents a heatmap comparing binders and mastic-extracted under fresh, short-term aging (STA), and long-term aging (LTA) conditions. Extracted binders at fresh and STA conditions are closely aligned with short-term aged original binders, with a greater distance observed for binders

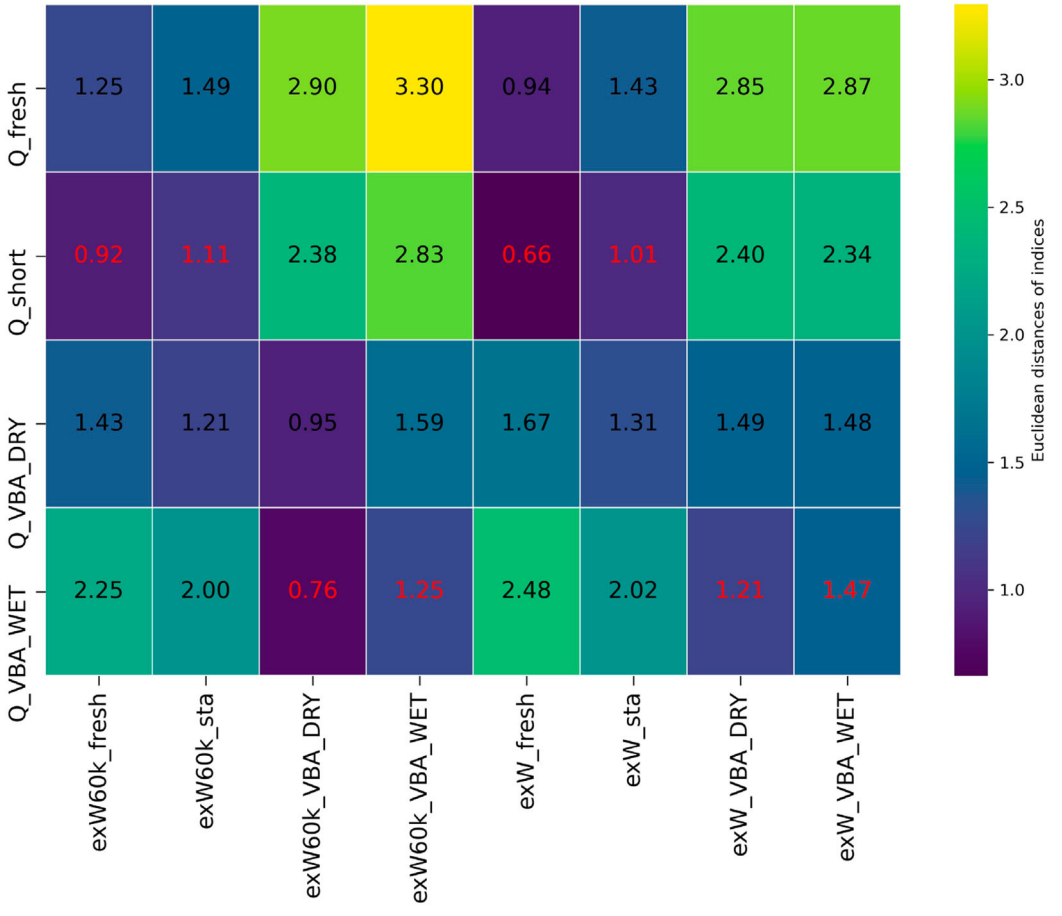

Figure 12. Heatmap of the Euclidean distance matrix used to evaluate the similarity in fresh, STA, and long-term aging (aged under VBA-DRY and VBA-WET) between binder and extracted binder from mastic samples. A smaller value indicates more similar chemical properties under specific aging conditions, reflecting the closeness of those conditions at either the binder or mixture level.

extracted from STA-aged mastics. This is due to the additional aging in mastics caused by the sample preparation and binder extraction processes. For all VBA-aged mastic samples, the corresponding extracted binders show closer proximity to binders aged under VBA-WET conditions instead of VBA-DRY conditions, with higher distance values observed for the extracted binder from VBA-WET mastics. This trend reflects the amplified aging effects observed in VBA-WET environments, where humidity plays a key role in accelerating oxidative processes. Additionally, the binder from W mastic is farther away from Q-VBA-WET compared to W60k mastic, suggesting a potential anti-aging effect of hydrated lime.

For the comparison of mixture and binder samples, since aging at a high pressure of 150 bar is not commonly used or practical, only aging at 1 bar is considered. Figure 13 displays the heatmap comparing binder samples to mixture samples. For all PA mixture samples hygrothermally aged at 1 bar for 3 weeks at various temperatures, the closest binder aging condition is hygrothermal aging at 60°C. Similarly, for all SMA mixture samples hygrothermally aged at 1 bar for 3 weeks, the closest binder aging condition is hygrothermal aging at 70°C. This indicates that SMA samples experience slightly more aging than PA samples, consistent with the trends observed in the sulfoxide and aliphatic index. It is important to note that while binder ageing conditions cannot yield identical chemical changes in mixtures, as indicated by the non-zero distance values and the differences in FTIR indices, it is possible

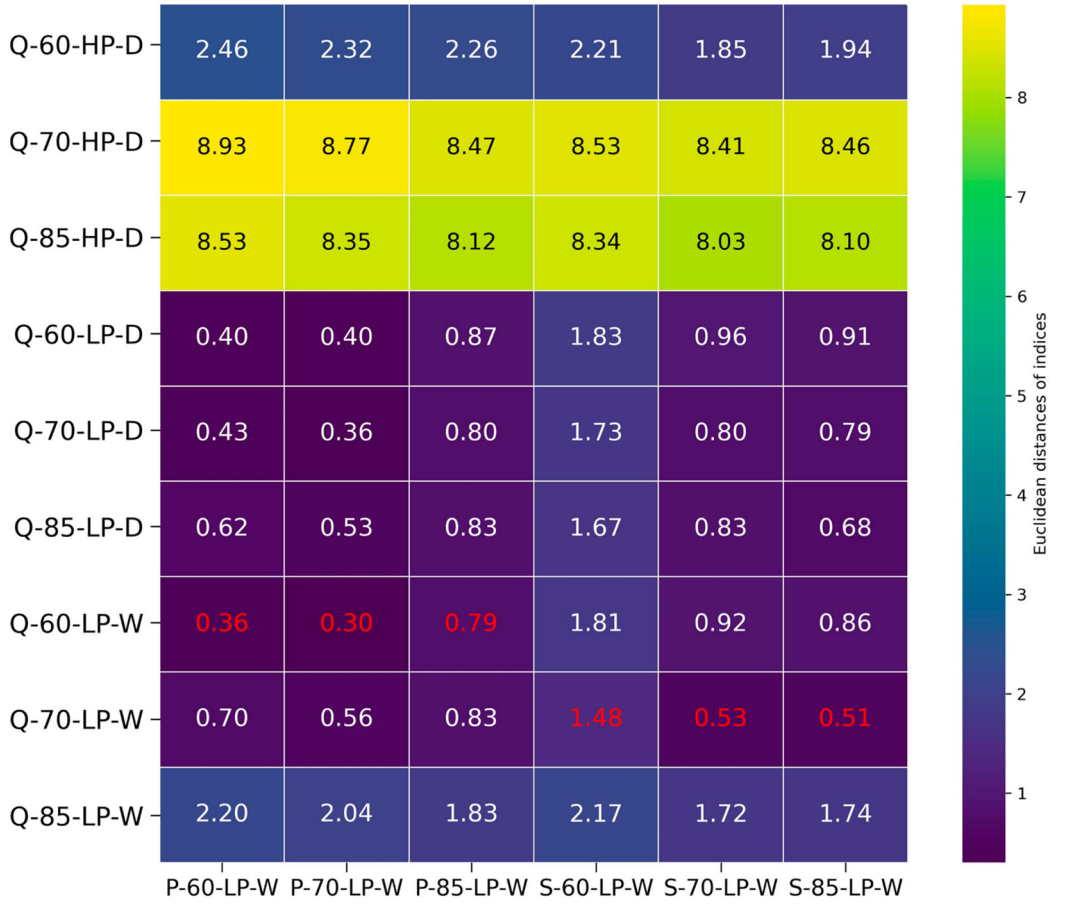

Figure 13. Heatmap of the Euclidean distance matrix used to evaluate the similarity in long-term aging between binder and mixture samples aged under the same pressure of 1 bar but different temperatures and humidities. A smaller value indicates more similar chemical properties between two samples, reflecting their closer ageing levels.

to identify binder ageing conditions that result in similar aging behaviour as observed in mixtures aged at either the same or different temperature and humidity conditions.

6. Conclusion

This study aimed to investigate the aging response of bituminous materials at different scales, namely, binders, mastics (with hydrated lime or limestone), and mixtures (PA or SMA), and assess the effectiveness of FTIR indices in characterising and comparing their ageing mechanisms. Specifically, the paper evaluates how temperature, pressure, humidity, and reactive oxygen species (ROS) influence aging at various material scales. Additionally, it aimed to determine if closely matching aging conditions could be identified across multi-scale samples and to examine the limitations of using binder-level aging data to predict behaviour in more complex systems like mastics and mixtures.

Results show that the advanced ATR correction effectively addressed the distortion of relative peak intensities, particularly at lower wavenumbers, and improved the reproducibility of the spectra. Nonetheless, the FTIR indices and their trends of change remain unaffected by the ATR correction. FTIR indices, while useful for tracking chemical changes, were significantly affected by the presence filler in mastics, complicating direct comparisons between mastics and binders using FITR results.

For mastic samples, the type of fillers significantly affects their ageing behaviour. Mastics with hydrated lime showed improved resistance to oxidative aging, especially under humid conditions, where hydrated lime reduced carbonyl formation and preserved hydroxyl functionality. Compared to binders, mastics reveal different FTIR results. The interactions between fillers and binders made mastic and binder aging processes distinct, suggesting that binder studies alone are insufficient for predicting mastic behaviour especially for mastics with active fillers. The PCA analysis further emphasised this distinction, showing clear separation in the spectral data of mastics and binders.

Mixture samples aged under conditions similar to binder aging exhibited comparable chemical changes to binders, with PA mixtures showing more susceptibility to aging at lower temperatures and pressures (which are similar to field aging condition), while SMA mixtures experienced more laboratory aging at extremely harsh conditions due to their denser structure. Environmental factors such as temperature, pressure, and humidity significantly impacted aging, particularly through oxidative pathways marked by increases in carbonyl and sulfoxide indices.

Moreover, the study utilised a Euclidean distance matrix to quantify the divergence in aging processes between binder, mastic, and mixture samples. The analysis showed that the aging of binders and mastics, while distinct due to filler effects, exhibited some comparability, particularly when hydrated lime was involved Mastics containing hydrated lime aged under wet conditions (VBA-WET) showed closer proximity to similarly aged binders than those with limestone fillers. The study also demonstrated that binder samples aged at 1 bar pressure shared significant chemical similarities with mixtures aged under the same conditions. For PA mixtures, the closest comparable aging condition in binders occurred at 60°C, while for SMA mixtures, it was 70°C, indicating that binder-level aging can approximate mixture aging at lower pressures. Overall, binder-level tests, particularly at low pressures, were found to better capture the aging dynamics in mixtures with minor nuances.

In conclusion, while binder aging cannot fully capture the complexity of aging at mastic and mixture scales, it provides valuable insights into the aging at these scales. FTIR indices are effective for tracking aging at various scales but require tailored interpretations when fillers are present. The Euclidean distance analysis highlights the similarities and differences across material scales, indicating that binder-level studies can offer partial predictions for mastic and mixture aging under specific conditions. Future work should focus on refining FTIR analysis techniques for mastics and developing more precise methods for studying aging processes in multi-scale asphalt systems to better understand the interplay between binders, fillers, microstructure, and environmental factors.

Acknowledgements

This paper/article is created under the research programme Knowledge based Pavement Engineering (KPE, funded by Rijkswaterstaat, contract number = 31164321). KPE is a cooperation between Rijkswaterstaat, TNO and TU Delft in which scientific and applied knowledge is gained about asphalt pavements and which contributes to the aim of Rijkswaterstaat to be completely climate neutral and to work according to the circular principle by 2030. The opinions expressed in this paper is solely from the authors. The financial support by the Austrian Federal Ministry for Digital and Economic Affairs, the National Foundation for Research, Technology and Development and the Christian Doppler Research Association is gratefully acknowledged. The authors would also like to express their gratitude to the CD laboratory company partners BMI Group, OMV Downstream and Pittel + Brausewetter for their financial support. AV also acknowledges NWO-AES (Dutch Research Council) for a Talent Programme VENI grant (number: 18148) for the project 'A multiscale approach towards future road infrastructure: How to design sustainable paving materials?'

Disclosure statement

No potential conflict of interest was reported by the author(s).

Funding

This work was supported by Austrian Federal Ministry for Digital and Economic Affairs, the National Foundation for Research, Technology and Development: [Grant Number]; CD laboratory company partners BMI Group, OMV Downstream and Pittel + Brausewetter: [Grant Number]; NWO-AES: [Grant Number 18148]; Rijkswaterstaat: [Grant Number 31164321].

ORCID

Kristina Primerano http://orcid.org/0000-0001-5978-1989
Johannes Mirwald http://orcid.org/0000-0001-5025-7427
Bernhard Hofko http://orcid.org/0000-0002-8329-8687
Aikaterini Varveri http://orcid.org/0000-0002-8830-9437

References

Airey, G. D. (2003). State of the art report on ageing test methods for bituminous pavement materials. *International Journal of Pavement Engineering*, *4*(3), 165–176. https://doi.org/10.1080/1029843042000198568

Alfaqawi, R. M., Fareed, A., Zaidi, S. B. A., Airey, G. D., & Rahim, A. (2022). Effect of hydrated lime and other mineral fillers on stiffening and oxidative ageing in bitumen mastic. *Construction and Building Materials*, *315*, 125789. https://doi.org/10.1016/j.conbuildmat.2021.125789

Anderson, D., Bahia, H., & Dongre, R. (1992). *Rheological properties of mineral filler-asphalt mastics and its importance to pavement performance*. ASTM International.

Domazet-Lošo, M., & Haubold, B. (2009). Efficient estimation of pairwise distances between genomes. *Bioinformatics (oxford, England)*, *25*(24), 3221–3227.

EN 12607-1, C. (2014). 12607-1: Bitumen and Bituminous Binders—Determination of the Resistance to Hardening under Influence of Heat and Air—Part 1: RTFOT Method. *European Committee for Standardization: Brussels, Belgium*.

EN 14769, C. (2012). 14769: Bitumen and Bituminous Binders—Accelerated Long-Term Ageing Conditioning by a Pressure Ageing Vessel (PAV). *European Committee for Standardization: Brussels, Belgium*.

Erkens, S., Porot, L., Glaser, R., & Glover, C. J. (2016). Aging of bitumen and asphalt concrete: Comparing state of the practice and ongoing developments in the United States and Europe. Transportation research board 95th annual meeting, Transportation Research Board (TRB).

Filonzi, A., Lee, S. K., Ferreira, W., Hajj, R., & Bhasin, A. (2020). A micro-extraction method for use with 4 mm plate geometry in the dynamic shear rheometer to evaluate asphalt binder rheology. *Construction and Building Materials*, *252*, 119024. https://doi.org/10.1016/j.conbuildmat.2020.119024

Gubler, R., Liu, Y., Anderson, D. A., & Partl, M. N. (1999). Investigation of the system filler and asphalt binders by rheological means. *Journal of the Association of Asphalt Paving Technologists*, *68*.

Highways, A. A. o. S., & Officials, T. (1994). *Practice for short and long term ageing of hot mix asphalt*. AASHTO Designation PP2.

Hofer, K., Werkovits, S., Schönauer, P., Mirwald, J., Grothe, H., & Hofko, B. (2023). Chemical and mechanical analysis of field and laboratory aged bitumen. *Road Materials and Pavement Design*, *24*(sup1), 160–175. https://doi.org/10.1080/14680629.2023.2180297

Hofko, B., & Hospodka, M. (2016). Rolling thin film oven test and pressure aging vessel conditioning parameters: Effect on viscoelastic behavior and binder performance grade. *Transportation Research Record*, *2574*(1), 111–116. https://doi.org/10.3141/2574-12

Hofko, B., Maschauer, D., Steiner, D., Mirwald, J., & Grothe, H. (2020). Bitumen ageing–Impact of reactive oxygen species. *Case Studies in Construction Materials*, *13*, e00390. https://doi.org/10.1016/j.cscm.2020.e00390

Hofko, B., Porot, L., Falchetto Cannone, A., Poulikakos, L., Huber, L., Lu, X., Mollenhauer, K., & Grothe, H. (2018). FTIR spectral analysis of bituminous binders: Reproducibility and impact of ageing temperature. *Materials and Structures*, *51*(2), 1–16. https://doi.org/10.1617/s11527-018-1170-7

Hu, Y., Si, W., Kang, X., Xue, Y., Wang, H., Parry, T., & Airey, G. D. (2022). State of the art: Multiscale evaluation of bitumen ageing behaviour. *Fuel*, *326*, 125045. https://doi.org/10.1016/j.fuel.2022.125045

Jing, R. (2019). Ageing of bituminous materials: Experimental and numerical characterization.

Jing, R., Varveri, A., Liu, X., Scarpas, A., & Erkens, S. (2019). Laboratory and field aging effect on bitumen chemistry and rheology in porous asphalt mixture. *Transportation Research Record*, *2673*(3), 365–374. https://doi.org/10.1177/0361198119833362

Jing, R., Varveri, A., Liu, X., Scarpas, A., & Erkens, S. (2021). Ageing effect on chemo-mechanics of bitumen. *Road Materials and Pavement Design*, *22*(5), 1044–1059. https://doi.org/10.1080/14680629.2019.1661275

Jing, R., Varveri, A., Liu, X., Scarpas, A., & Erkens, S. (2022). Ageing Behavior of Porous and Dense Asphalt Mixtures in the Field. Proceedings of the RILEM International Symposium on Bituminous Materials: ISBM Lyon 2020 1, Springer.

Khalighi, S., Erkens, S., & Varveri, A. (2024a). Exploring the impact of humidity and water on bituminous binder aging: A multivariate analysis approach (TI CAB). *Road Materials and Pavement Design*, 1–25. https://doi.org/10.1080/14680629.2024.2364189

Khalighi, S., Jing, R., Varveri, A., & Erkens, S. (2024d). Exploring the significance of exposed surface area in the aging of bitumen films with equal thickness. *Bituminous Mixtures and Pavements, VIII*, CRC Press**:** 71–79.

Khalighi, S., Ma, L., Mosleh, Y., van Lent, D., & Varveri, A. (2024b). Multivariate chemo-rheological framework for optimizing laboratory aging protocols of paving binders. *Materials & Design*, *248*, 113520. https://doi.org/10.1016/j.matdes.2024.113520

Khalighi, S., Ma, L., Ren, S., & Varveri, A. (2024c). Evaluating the impact of data pre-processing methods on classification of ATR-FTIR spectra of bituminous binders. *Fuel*, *376*, 132701. https://doi.org/10.1016/j.fuel.2024.132701

khalighi, S., Ma, L., & Varveri, A. (2025a). Novel Accelerated Photodecomposition-Induced Aging with Hydrogen Peroxide for Bituminous Binders, Available at SSRN 5106244.

Khalighi, S., Primerano, K., Mirwald, J., Hofko, B., & Varveri, A. (2025b). The impact of reactive oxygen species coupled with moisture on bitumen long-term aging. *Road Materials and Pavement Design*, 1–20. https://doi.org/10.1080/14680629.2024.2364189

Koyun, A., Büchner, J., Wistuba, M. P., & Grothe, H. (2022). Rheological, spectroscopic and microscopic assessment of asphalt binder ageing. *Road Materials and Pavement Design*, *23*(1), 80–97. https://doi.org/10.1080/14680629.2020.1820891

Ma, L., Salehi, H. S., Jing, R., Erkens, S., Vlugt, T. J., Moultos, O. A., Greenfield, M. L., & Varveri, A. (2023a). Water diffusion mechanisms in bitumen studied through molecular dynamics simulations. *Construction and Building Materials*, *409*, 133828. https://doi.org/10.1016/j.conbuildmat.2023.133828

Ma, L., Varveri, A., Jing, R., & Erkens, S. (2023b). Chemical characterisation of bitumen type and ageing state based on FTIR spectroscopy and discriminant analysis integrated with variable selection methods. *Road Materials and Pavement Design*, 24(sup1), 1–15.

Maschauer, D., Mirwald, J., & Hofko, B. (2022). Viennese Ageing Procedure (VAPro): adaptions and further development to address low-temperature performance of aged asphalt mixtures. *Road Materials and Pavement Design*, *23*(sup1), 147–161. https://doi.org/10.1080/14680629.2022.2029547

Maschauer, D., Steiner, D., Mirwald, J., & Hofko, B. (2023). Chemical and mechanical analysis of VAPro-aged asphalt binders from different crude oil sources. *Materials and Structures*, *56*(9), 168. https://doi.org/10.1617/s11527-023-02249-y

Mayerhöfer, T. G., Ilchenko, O., Kutsyk, A., & Popp, J. (2022). Beyond beer's law: Quasi-ideal binary liquid mixtures. *Applied Spectroscopy*, *76*(1), 92–104. https://doi.org/10.1177/00037028211056293

Mirwald, J., Maschauer, D., Hofko, B., & Grothe, H. (2020). Impact of reactive oxygen species on bitumen aging–The viennese binder aging method. *Construction and Building Materials*, *257*, 119495. https://doi.org/10.1016/j.conbuildmat.2020.119495

Mirwald, J., Nura, D., & Hofko, B. (2022). Recommendations for handling bitumen prior to FTIR spectroscopy. *Materials and Structures*, *55*(2), 26. https://doi.org/10.1617/s11527-022-01884-1

Moraes, R., & Bahia, H. (2015). Effect of mineral fillers on the oxidative aging of asphalt binders: Laboratory study with mastics. *Transportation Research Record*, *2506*(1), 19–31. https://doi.org/10.3141/2506-03

Motevalizadeh, S. M., & Mollenhauer, K. (2024). Use of multivariate clustering analysis to investigate the physicochemical interactions in bitumen mastics using micromechanical modeling and FTIR spectroscopy. *Construction and Building Materials*, *448*, 138230. https://doi.org/10.1016/j.conbuildmat.2024.138230

Nagabhushanarao, S. S., & Vijayakumar, A. (2021). Chemical and rheological characteristics of accelerate aged asphalt binders using rolling thin film oven. *Construction and Building Materials*, *272*, 121995. https://doi.org/10.1016/j.conbuildmat.2020.121995

Nivitha, M., Prasad, E., & Krishnan, J. (2016). Ageing in modified bitumen using FTIR spectroscopy. *International Journal of Pavement Engineering*, *17*(7), 565–577. https://doi.org/10.1080/10298436.2015.1007230

Oliver, J., & Tredrea, P. (1997). The change in properties of polymer modified binders with simulated field exposure (With discussion). *Journal of the Association of Asphalt Paving Technologists*, *66*. https://trid.trb.org/View/488045

Petersen, J. C. (2009). A review of the fundamentals of asphalt oxidation: chemical, physicochemical, physical property, and durability relationships. *Transportation research circular*.(E-C140).

Plancher, H., Green, E., & Petersen, J. (1976). *Reduction of oxidative hardening of asphalts by treatment with hydrated lime–a mechanistic study*. Association of Asphalt Paving Technologists Proc.

Porot, L., Mouillet, V., Margaritis, A., Haghshenas, H., Elwardany, M., & Apostolidis, P. (2023). Fourier-transform infrared analysis and interpretation for bituminous binders. *Road Materials and Pavement Design*, *24*(2), 462–483. https://doi.org/10.1080/14680629.2021.2020681

Primerano, K., Mirwald, J., Lohninger, J., & Hofko, B. (2023). Characterization of long-term aged bitumen with FTIR spectroscopy and multivariate analysis methods. *Construction and Building Materials*, *409*, 133956. https://doi.org/10.1016/j.conbuildmat.2023.133956

Recasens, R. M., Martínez, A., Jiménez, F. P., & Bianchetto, H. (2005). Effect of filler on the aging potential of asphalt mixtures. *Transportation Research Record*, *1901*(1), 10–17. https://doi.org/10.1177/0361198105190100102

Ren, R., Han, K., Zhao, P., Shi, J., Zhao, L., Gao, D., Zhang, Z., & Yang, Z. (2019). Identification of asphalt fingerprints based on ATR-FTIR spectroscopy and principal component-linear discriminant analysis. *Construction and Building Materials*, *198*, 662–668. https://doi.org/10.1016/j.conbuildmat.2018.12.009

Schmidt, R. (1973). Laboratory measurement of the durability of paving asphalts. Viscosity Testing of Asphalt and Experience with Viscosity Graded Specifications, ASTM International.

Simon Nunn, K. N. (2008). Advanced ATR Correction Algorithm.

Singh, C. V., Pachauri, P., Dwivedi, S. P., Sharma, S., & Singari, R. (2022). Formation of functionally graded hybrid composite materials with Al2O3 and RHA reinforcements using friction stir process. *Australian Journal of Mechanical Engineering*, *20*(1), 141–154. https://doi.org/10.1080/14484846.2019.1679583

Siroma, R. S., Nguyen, M. L., Hornych, P., Lorino, T., & Chailleux, E. (2021). Clustering aged bitumens through multivariate statistical analyses using phase angle master curve. *Road Materials and Pavement Design*, *22*(sup1), S51–S68. https://doi.org/10.1080/14680629.2021.1907217

Sreeram, A., Masad, A., Nia, Z. S., Maschauer, D., Mirwald, J., Hofko, B., & Bhasin, A. (2021). Accelerated aging of loose asphalt mixtures using ozone and other reactive oxygen species. *Construction and Building Materials*, *307*, 124975. https://doi.org/10.1016/j.conbuildmat.2021.124975

Varveri, A., Avgerinopoulos, S., Kasbergen, C., Scarpas, A., & Collop, A. (2014). Influence of air void content on moisture damage susceptibility of asphalt mixtures: Computational study. *Transportation Research Record*, *2446*(1), 8–16. https://doi.org/10.3141/2446-02

Wang, K., Yuan, Y., Han, S., & Yang, H. (2018). Application of attenuated total reflectance Fourier transform infrared (ATR-FTIR) and principal component analysis (PCA) for quick identifying of the bitumen produced by different manufacturers. *Road Materials and Pavement Design*, *19*(8), 1940–1949. https://doi.org/10.1080/14680629.2017.1352016

Weigel, S., & Stephan, D. (2017). The prediction of bitumen properties based on FTIR and multivariate analysis methods. *Fuel*, *208*, 655–661. https://doi.org/10.1016/j.fuel.2017.07.048

Wu, W., Jiang, W., Yuan, D., Lu, R., Shan, J., Xiao, J., & Ogbon, A. W. (2021). A review of asphalt-filler interaction: Mechanisms, evaluation methods, and influencing factors. *Construction and Building Materials*, *299*, 124279. https://doi.org/10.1016/j.conbuildmat.2021.124279

Zhang, H., Zheng, F., Zhang, J., Hu, D., Minelli, M., Pei, J., & Sangiorgi, C. (2024). Contributions of Fourier-transform infrared spectroscopy technologies to the research of asphalt materials: A comprehensive review. *Fuel*, *371*, 132078. https://doi.org/10.1016/j.fuel.2024.132078